Inorganic Chemistry

pubs.acs.org/IC Article

# Hetero-Bis-Conjugation of Bioactive Molecules to Half-Sandwich Ruthenium(II) and Iridium(III) Complexes Provides Synergic Effects in Cancer Cell Cytotoxicity

Lorenzo Biancalana,* Hana Kostrhunova, Lucinda K. Batchelor, Mouna Hadiji, Ilaria Degano, Guido Pampaloni, Stefano Zacchini, Paul J. Dyson, Viktor Brabec,* and Fabio Marchetti

Cite This: *Inorg. Chem.* 2021, 60, 9529–9541 Read Online

ACCESS | Metrics & More | Article Recommendations | Supporting Information

**ABSTRACT:** Four bipyridine-type ligands variably derivatized with two bioactive groups (taken from ethacrynic acid, flurbiprofen, biotin, and benzylpenicillin) were prepared via sequential esterification steps from commercial 2,2′-bipyridine-4,4′-dicarboxylic acid and subsequently coordinated to ruthenium(II) *p*-cymene and iridium(III) pentamethylcyclopentadienyl scaffolds. The resulting complexes were isolated as nitrate salts in high yields and fully characterized by analytical and spectroscopic methods. NMR and MS studies in aqueous solution and in cell culture medium highlighted a substantial stability of ligand coordination and a slow release of the bioactive fragments in the latter case. The complexes were assessed for their antiproliferative activity on four cancer cell lines, showing cytotoxicity to the low micromolar level (equipotent with cisplatin). Additional biological experiments revealed a multimodal mechanism of action of the investigated compounds, involving DNA metalation and enzyme inhibition. Synergic effects provided by specific combinations of metal and bioactive fragments were identified, pointing toward an optimal ethacrynic acid/flurbiprofen combination for both Ru(II) and Ir(III) complexes.

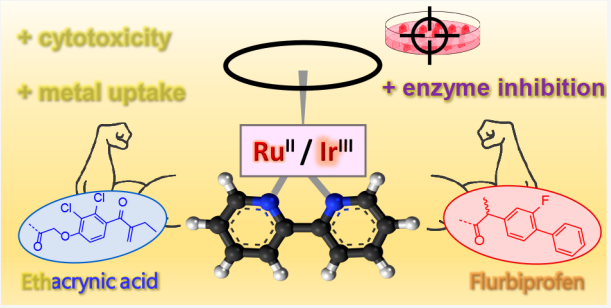


## INTRODUCTION

The conjugation of biologically active metal scaffolds and organic molecules is a well-documented strategy to enhance the therapeutic effects of the resulting compound and is widely applied to cytotoxic metal complexes investigated as potential anticancer agents.[1] In general, "bioactive molecules" are both those possessing a pharmacological function on their own (providing a *multiaction* compound) and those behaving as "vectors" for increasing the localization of a drug (providing a *targeted* compound). This approach to combine bioactive molecules with metal complexes met with success in several cases, where considerable synergic effects have been observed for the bioconjugates with respect to nonfunctionalized metal complexes and/or coadministration of the two individual components.[2] The mechanism of action of such derivatives is likely multimodal and often largely unknown, with respect to the interplay of the metal center and the bioactive ligands.

In this regard, the incorporation of *multiple* bioactive organic molecules on a monometallic structure is expected to further improve anticancer activity, particularly if the former are endowed with different (complementary) modes of action and cellular targets.[3] In the past few years, several platinum(IV) compounds of this kind have been prepared, featuring various combinations of fragments targeting specific enzymes, receptors, and cellular compartments as well as organic antineoplastic agents.[4] From a synthetic standpoint, these complexes are obtained by sequential derivatization of *trans* (axial) Pt−OH groups with ester or carbamate linkages from common Pt(IV) precursors (Scheme 1a). The anticancer activity of such multitargeted/multiaction derivatives has been extensively investigated; some of these were able to outperform reference platinum drugs in terms of cancer cell cytotoxicity and also in 3D cell cultures and activity against primary tumors *in vivo*.[4b−d4h]

Inspired by the same principle, we recently reported a series of platinum(II) complexes containing (hetero)bis-functionalized bipyridine ligands (Scheme 1b).[5] Complexes carrying ethacrynic acid and/or flurbiprofen (*vide infra*) displayed marked cytotoxicity with respect to cisplatin in retinoblastoma and ovarian cancer cell lines, along with improved cancer cell selectivity.

**Received:** March 3, 2021
**Published:** June 22, 2021

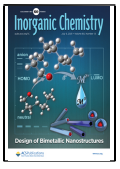






https://doi.org/10.1021/acs.inorgchem.1c00641
*Inorg. Chem.* 2021, 60, 9529−9541

**Scheme 1. General Structure of Platinum(IV) (a) and Platinum(II) (b) Complexes Conjugated with Two Different Bioactive Molecules Reported in the Literature and Bioactive Carboxylic Acids Employed in This Work (c)**

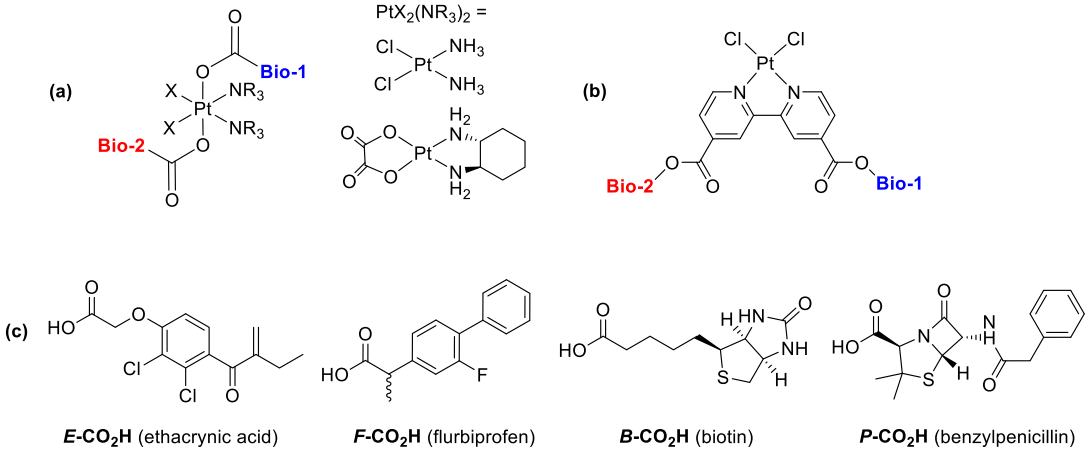


In light of these promising results, we decided to coordinate the bis-functionalized bipyridines to Ru(II) *p*-cymene and Ir(III) pentamethylcyclopentadienyl structures, which have been widely investigated for their anticancer potential.[6] Note that double functionalization with two different biofragments is quite rare for these metal scaffolds.[7] Four bioactive carboxylic acids were selected for the present work: *ethacrynic acid* (***E*-$CO_2H$**), *flurbiprofen* (***F*-$CO_2H$**), *biotin* (***B*-$CO_2H$**), and *benzylpenicillin* (***P*-$CO_2H$**) (Scheme 1c). Ethacrynic acid is an inhibitor of glutathione *S*-transferases (GST), enzymes that are implicated in resistance mechanisms in various cancer cell lines.[2a,8] Ruthenium arene complexes derivatized with ethacrynic acid typically are cytotoxic also in cisplatin-resistant cell lines,[9] whereas iridium−ethacrynic acid conjugates have not yet been reported. Cyclooxygenase enzymes (COX, especially COX-2) represent another important drug target, as they are upregulated in several human cancers.[10] Thus, a variety of nonsteroidal anti-inflammatory drugs—not including flurbiprofen—has been tethered to half-sandwich ruthenium and iridium complexes (mostly Ru) to investigate their anticancer activity.[11] Biotin (vitamin $B_{12}$) has been frequently introduced in the structure of metal complexes, aiming to assist their cellular uptake, taking advantage of the overexpression of vitamin receptors.[7b,12] In this regard, several biotinylated Ir($\eta^5$-Cp*) derivatives have been investigated within the field of artificial metalloenzymes, but not in view of their possible anticancer activity.[13]

Benzylpenicillin was considered with a view to expand the panel of bioactive fragments of interest in the design of anticancer metal complexes. As a matter of fact, transition-metal conjugates with *β*-lactam antibiotics (ampicillin, penicillin, and related species) are sparse and have been mostly studied for their antibacterial activity.[14]

The cytotoxicity of herein reported hetero(bis)conjugated Ru and Ir complexes was investigated against ovarian, breast, and cervical cancer cell lines, these cancers being currently treated using combination chemotherapy involving platinum and/or organic drugs.[15]

## RESULTS AND DISCUSSION

**Synthesis and Characterization.** Derivatization of 2,2′-bipyridine-4,4′-dicarboxylic acid with ethylene glycol followed by Steglich esterification/silica chromatography steps afforded the heterofunctionalized ligands containing ethacrynic acid and flurbiprofen ($\mathbf{L}^{EF}$) or biotin ($\mathbf{L}^{EB}$), according to the recently reported procedure (Scheme 2a).[5] A different strategy was adopted for the functionalization with benzylpenicillin, since a clean conversion of the commercially available potassium salt into the carboxylic acid was not effective. Thus, the bipyridine diacid was first converted into its 2-chloroethyl diester and the latter was allowed to react with an excess of potassium benzylpenicillin in DMF at 85 °C, to afford the desired compound ($\mathbf{L}^{PP}$; Scheme 2b). Subsequently, treatment of $[RuCl_2(\eta^6\text{-}p\text{-cymene})]_2$ or $[IrCl_2(\eta^5\text{-}C_5Me_5)]_2$ with $AgNO_3$ in MeCN followed by reaction with the appropriate bipyridine ligand at reflux afforded the complexes $[RuCl(\eta^6\text{-}p\text{-cymene})(\kappa^2N\text{-}\mathbf{L})]^+$ and $[IrCl(\eta^5\text{-}C_5Me_5)(\kappa^2N\text{-}\mathbf{L})]^+$, respectively ($\mathbf{L}^{EF}$, $[\mathbf{1,2}]^+$; $\mathbf{L}^{EB}$, $[\mathbf{3,4}]^+$; $\mathbf{L}^{PP}$, $[\mathbf{5}]^+$; Scheme 2c). The reaction of bipyridine ligands ($\mathbf{L}^{EF}$, $\mathbf{L}^{EB}$) with the iridium dimer in chloroform under reflux and subsequent $Cl^-/NO_3^-$ exchange was also effective (Scheme 2d). Dimethyl[2,2′-bipyridine]-4,4′-dicarboxylate ($\mathbf{L}^{MeMe}$) was synthesized according to a literature method[16] and used to obtain $[\mathbf{6}]^+$ and $[\mathbf{7}]^+$ as reference compounds. All reactions were carried out under stoichiometric conditions, and the Ru/Ir complexes were isolated as their nitrate salts in 83−95% yield, without the need for purification. The air- and moisture-stable ocher yellow (Ru) and orange (Ir) solids are soluble in polar organic solvents (e.g., DMSO, MeCN, $CH_2Cl_2$) but poorly soluble in water. To the best of our knowledge, the series of complexes $[\mathbf{1-5}]^+$ includes the first cases of iridium and ruthenium compounds derivatized with flurbiprofen or benzylpenicillin[17] and also the first iridium−ethacrynic acid conjugate.

The novel compounds were characterized by analytical (CNH analysis), spectroscopic (solid-state IR, multinuclear and bidimensional NMR), and high-resolution MS spectrometry techniques (see Figures S1−S33 in the Supporting Information). In addition, the crystal structure of $[\mathbf{6}]BF_4$ (obtained by $[\mathbf{6}]NO_3$ + $NaBF_4$ metathesis) was confirmed by X-ray diffraction (see Figure S34 and Table S1).[18]

The IR spectra of $[\mathbf{1-5}]NO_3$ (in the solid state) display strong bands in the region 1760−1730 $cm^{-1}$ accounting for the ester groups, along with other nearby C═O stretching absorptions. For instance, the bis-penicillin ester $\mathbf{L}^{PP}$ and the corresponding Ru(II) derivative $[\mathbf{5}]NO_3$ show an additional intense band at 1780 $cm^{-1}$ due to the *β*-lactam ring. The NMR spectra of $[\mathbf{1-4}]NO_3$ contain two sets of signals, often overlapping; this effect is especially noticeable for $^1H/^{13}C$


https://doi.org/10.1021/acs.inorgchem.1c00641
Inorg. Chem. 2021, 60, 9529−9541

**Scheme 2. Structures and Synthetic Routes for Bipyridine Ligands Derivatized with Ethacrynic Acid (*E*-$CO_2H$), Flurbiprofen (*F*-$CO_2H$), biotin (*B*-$CO_2H$), and Benzylpenicillin (*P*-$CO_2H$) and the Respective Ruthenium(II) *p*-Cymene and Iridium(III) Pentamethylcyclopentadienyl Complexes[a]**

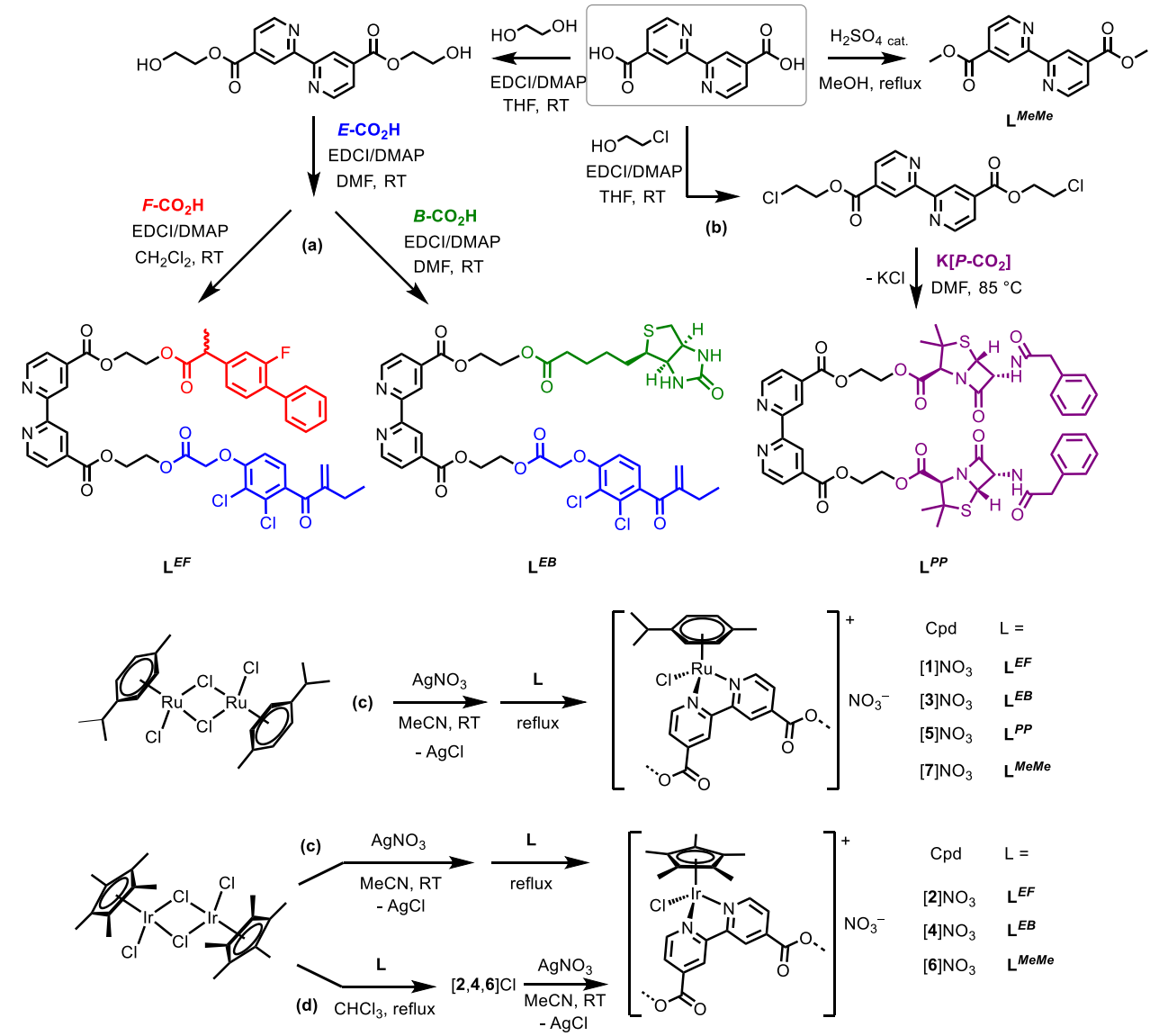


[a]RT = room temperature.

NMR signals related to the bipyridine rings as well as in $^{19}F$ NMR spectra of [**1**,**2**]$NO_3$. Indeed, the asymmetry of bipyridine ligands $\mathbf{L}^{EB}$ and $\mathbf{L}^{EF}$ results in a chiral metal center and therefore complexes $[\mathbf{1},\mathbf{2}]^+$ were obtained as a (racemic) mixture of diastereomers. On the other hand, [**5**]$NO_3$ exists as a single diastereomer, in which the doubling of NMR signals is due to diastereotopic atoms (e.g., the CH protons of the *p*-cymene ligand). Accordingly, [**6**,**7**]$NO_3$ display symmetric, achiral bipyridine ligands, giving rise to a single set of signals. The nitrate anion in [**1**−**7**]$NO_3$ manifests itself with a strong IR absorption around 1330 $cm^{-1}$ and a $^{14}N$ NMR resonance occurring in the −1.5 to +3.5 ppm range.

**Behavior in Aqueous Solution and Cell Culture Medium.** A preliminary assessment of the stability of ruthenium and iridium complexes in an aqueous medium[19] was carried out on 10 mM solutions in DMSO-$d_6$/$D_2O$ 5/1 v/v at 37 °C by $^1H$ NMR. Under these conditions, all compounds were completely inert over 72 h (≥96% stability; Figures S35−S39). The release of organic fragments, resulting from ligand dissociation and/or ester hydrolysis, was ruled out by comparison with the respective $^1H$ NMR spectrum. Next, in order to check for metal chloride solvolysis, a stoichiometric amount of $Ag(CF_3SO_3)$ was added to $[\mathbf{6}]^+$ and $[\mathbf{7}]^+$. Partial or complete conversion of the starting material required heating at 50 °C for 3−5 h (Figures S40 and S41); a spectral comparison before and after reaction with $Ag(CF_3SO_3)$ allowed unambiguous assignment of the set of signals to the parent chloro ($[\mathbf{6}]^+$, $[\mathbf{7}]^+$) and solvato ($[\mathbf{6}^S]^{2+}$, $[\mathbf{7}^S]^{2+}$) complexes (Scheme S1). Nevertheless, hydrolysis of metal−chloride bonds on half-sandwich Ru(II) and Ir(III) 2,2′-bipyridine complexes should be facilitated on increasing the dilution and water content of the medium.[20]

In contrast, transesterification processes are triggered upon dissolution in methanol at room temperature, as ascertained by NMR spectroscopy and MS spectrometry (see the Experimental Section and the Supporting Information). Such


https://doi.org/10.1021/acs.inorgchem.1c00641
Inorg. Chem. 2021, 60, 9529−9541

reactivity was previously observed for the bipyridines $\mathbf{L}^{EF}$ and $\mathbf{L}^{EB}$ and their Pt(II) complexes.[5] In the case of $[\mathbf{1}-\mathbf{4}]^+$, methanolysis occurs predominantly at the bipyridine-bound carboxyl, leading to the release of the 2-hydroxyethyl esters of ethacrynic acid, flurbiprofen, and biotin. For comparison, the $\mathbf{L}^{MeMe}$ derivatives $[\mathbf{6},\mathbf{7}]^+$ are much more inert, indicating that the steric bulk of bioconjugated 2,2′-bipyridine ligands favors ester cleavage.

Next, the stability of ruthenium and iridium complexes under physiologically relevant conditions was investigated. Therefore, 40 $\mu$M solutions of $[\mathbf{1}-\mathbf{5}]NO_3$ in RPMI cell culture medium (1% DMSO; pH ∼7.4) were incubated at 37 °C for variable times (0/24/48 h) and then analyzed by HPLC-MS. The parent organometallic cation was observed in solution in each case, along with fragments derived from the hydrolysis of ester bonds. In this respect, the release of benzylpenicillin and the four 2-hydroxyethyl esters could not be quantified, due to matrix effects that have not been clarified. Conversely, the percentage amounts of ethacrynic acid, biotin, and flurbiprofen (carboxylates) released over time are reported in Table 1.

**Table 1. Percentages of Ethacrynic Acid, Biotin, and Flurbiprofen Carboxylates Released from Solutions of $[\mathbf{1}-\mathbf{4}]^+$ in RPMI Cell Culture Medium (ca. 40 $\mu$M, 1% DMSO, pH ∼7.4) at 37 °C for Different Incubation Times (0−48 h)**

| | % *E*-$CO_2$H released[a] | | | % *F*-$CO_2$H or *B*-$CO_2$H released[a,b] | | |
|---|---|---|---|---|---|---|
| compound | 0 h | 24 h | 48 h | 0 h | 24 h | 48 h |
| $[\mathbf{1}]NO_3$ | 6 | 4 | 3 | 0 | 0 | 0 |
| $[\mathbf{2}]NO_3$ | 12 | 14 | 8 | 0 | 0 | 0 |
| $[\mathbf{3}]NO_3$ | 34 | 33 | 28 | 9 | 29 | 51 |
| $[\mathbf{4}]NO_3$ | 39 | 28 | 26 | 10 | 40 | 64 |

[a]Starting concentrations of the complexes were in the range 33−41 $\mu$M. The analytical blank did not contain any relevant amount of the analytes. The CV% was below 10%. [b]% ***F*-$CO_2$H** for $[\mathbf{1},\mathbf{2}]^+$; % ***B*-$CO_2$H** for $[\mathbf{3},\mathbf{4}]^+$.

Complexes $[\mathbf{1}]^+$ and $[\mathbf{2}]^+$ readily produce a minor amount (6−12%) of ethacrynic acid, which decreases after 48 h, possibly due to its degradation. No flurbiprofen was found in solution above the quantitation limit (0.4 $\mu$M) at any incubation time. A consistent amount of ethacrynic acid quickly detaches from both $[\mathbf{3}]^+$ and $[\mathbf{4}]^+$ (35−40%), and more than half of the biotin was found in solution after 48 h.

In conclusion, the stability experiments highlighted that Ru(II) and Ir(III) complexes $[\mathbf{1}-\mathbf{5}]^+$ possess a robust ligand set around the metal center but are susceptible to ester hydrolysis in the cell culture medium, leading to the progressive release of their bioactive organic cargo (in the form of carboxylates or 2-hydroxyethyl esters), thus behaving as prodrugs. Indeed, the aforementioned 2-hydroxyethyl esters might be biologically active themselves (e.g., in terms of enzyme inhibition or anticancer activity[21]) or undergo a subsequent hydrolysis to release the bioactive carboxylate. The timing of ester cleavage may affect their biological activity (*vide infra*).

**Cytotoxicity, Cellular Uptake, DNA Metalation, and Enzyme Inhibition.** The antiproliferative activity of complexes $[\mathbf{1}-\mathbf{7}]^+$ was determined in four human cancer cell lines (A2780, A2780cisR ovarian ± cisplatin-resistant, MCF-7 breast, and HeLa cervical) and nontumorigenic human embryonic kidney cells (HEK293), following 72 h incubation. $IC_{50}$ data are compiled in Table 2 with cisplatin, RAPTA-C, bipyridine ligands ($\mathbf{L}^{EF}$, $\mathbf{L}^{EB}$, $\mathbf{L}^{PP}$), and the bioactive carboxylic acids as reference compounds. Ethacrynic acid derivatized compounds $[\mathbf{1}-\mathbf{4}]^+$ are potent cytotoxic agents in the panel of cell lines, with $IC_{50}$ values ranging from 2.8 to 40 $\mu$M. The compounds are particularly effective on MCF-7 cells (in comparison to cisplatin) and on the cisplatin-resistant A2780cisR cell line, with resistance factors below 2.2 (vs 7 for cisplatin). Conversely, benzylpenicillin conjugates $[\mathbf{5}]NO_3$ and $\mathbf{L}^{PP}$ are essentially nontoxic in all cell lines.

Interestingly, some cytotoxicity trends on varying the nature of the metal center (Ru/Ir) and the organic fragments can be delineated. First, each iridium complex ($[\mathbf{2}]^+/[\mathbf{4}]^+/[\mathbf{6}]^+$) is

**Table 2. $IC_{50}$ values ($\mu$M) on Human Ovarian (A2780 and A2780cisR), Breast (MCF-7), and Cervical (HeLa) Cancer Cells and Human Embryonic Kidney (HEK-293) Cells after 72 h Incubation[a]**

| compound(s) | metal/bioactive fragments | A2780 | A2780cisR | MCF-7 | HeLa | HEK293 |
|---|---|---|---|---|---|---|
| $[\mathbf{1}]NO_3$ | Ru/ethacrynic acid/flurbiprofen | 5.6 ± 0.6 | 8.0 ± 0.7 | 10.6 ± 0.8 | 28 ± 4 | 7.3 ± 0.9 |
| $[\mathbf{2}]NO_3$ | Ir/ethacrynic acid/flurbiprofen | 2.8 ± 0.4 | 6.4 ± 0.5 | 8.0 ± 0.9 | 17.1 ± 0.6 | 10.3 ± 0.6 |
| $[\mathbf{3}]NO_3$ | Ru/ethacrynic acid/biotin | 11 ± 3 | 11 ± 2 | 22 ± 1 | 40 ± 6 | 9 ± 4[f] |
| $[\mathbf{4}]NO_3$ | Ir/ethacrynic acid/biotin | 7.0 ± 0.8 | 8.5 ± 0.5 | 9 ± 1 | 24 ± 5 | 12.5 ± 0.8 |
| $[\mathbf{5}]NO_3$ | Ru/benzylpenicillin (×2) | >200 | >200 | 270 ± 30 | 190 ± 10 | >200[f] |
| $[\mathbf{6}]NO_3$ | Ir/− | >100 | 63 ± 6 | 140 ± 30 | 190 ± 9 | >100[f] |
| $[\mathbf{7}]NO_3$ | Ru/− | >100 | >100 | 310 ± 40 | 220 ± 20 | >100 |
| $\mathbf{L}^{EF}$ | −/ethacrynic acid/flurbiprofen | >200 | >200 | >200 | >200 | >200 |
| $\mathbf{L}^{EB}$ | −/ethacrynic acid/biotin | 12 ± 1 | 16 ± 1 | 17 ± 2 | 14 ± 2 | 25 ± 2 |
| $\mathbf{L}^{PP}$ | −/benzylpenicillin (×2) | >200 | >200 | >200 | >200 | >200 |
| ethacrynic acid[b] | | 40 ± 3 | 53 ± 5 | 47 ± 4 | 56 ± 9 | 39 ± 1 |
| flurbiprofen | | >200 | >200 | 190 ± 30 | 200 ± 50 | >200 |
| benzylpenicillin[c] | | >200 | >200 | >200 | >200 | >200 |
| $[\mathbf{6}]NO_3$ + *E*-$CO_2$H + *F*-$CO_2$H[d] | Ir/ethacrynic acid/flurbiprofen | 34 ± 2 | 35 ± 2 | - | - | 37 ± 3 |
| $[\mathbf{7}]NO_3$ + *E*-$CO_2$H + *F*-$CO_2$H[d] | Ru/ethacrynic acid/flurbiprofen | 27 ± 3 | 39 ± 3 | - | - | 36 ± 2 |
| cisplatin | | 2.1 ± 0.4 | 15 ± 1 | 14.8 ± 0.9 | 15 ± 3 | 5.3 ± 0.7 |
| RAPTA-C[e] | | >200 | >200 | - | - | >200 |

[a]Values are given as mean ± SD. [b]Data for A2780/A2780cisR and HEK293 taken from ref 9c. [c]As the $K^+$ salt. [d]Coadministration of the compounds in a 1:1:1 molar ratio. [e]$[RuCl_2(\eta^6\text{-}p\text{-cymene})(\kappa P\text{-}1,3,5\text{-triaza-7-phosphaadamantane})]$. [f]Tested on HEK-293T cells.



https://doi.org/10.1021/acs.inorgchem.1c00641
Inorg. Chem. 2021, 60, 9529−9541

**Table 3. Cellular Uptake of Ru or Ir in A2780 Cells Treated with 5 or 10 $\mu$M of $[1-7]NO_3$ for 8 or 24 h and DNA Metalation in A2780 Cells Treated with 10 $\mu$M of $[1-7]NO_3$ for 24 h**

| | | cellular uptake (pmol Ru(Ir)/$10^6$ cells) | | | |
|---|---|---|---|---|---|
| compound | metal/bioactive fragments | 10 $\mu$M/8 h | 5 $\mu$M/24 h | 10 $\mu$M/24 h | DNA metalation (fmol Ru(Ir)/$\mu$g DNA) |
| $[\mathbf{1}]NO_3$ | Ru/ethacrynic acid/flurbiprofen | 88 ± 7 | 65 ± 9 | 130 ± 9 | 52 ± 9 (21 ± 7)[a] |
| $[\mathbf{2}]NO_3$ | Ir/ethacrynic acid/flurbiprofen | 61 ± 7 | 46 ± 6 | 100 ± 10 | 36 ± 3 (16 ± 3)[a] |
| $[\mathbf{3}]NO_3$ | Ru/ethacrynic acid/biotin | 9 ± 1 | 7 ± 2 | 13 ± 4 | 5.0 ± 0.9 |
| $[\mathbf{4}]NO_3$ | Ir/ethacrynic acid/biotin | 11 ± 2 | 8 ± 2 | 17 ± 4 | 12 ± 2 |
| $[\mathbf{5}]NO_3$ | Ru/benzylpenicillin (×2) | 4.6 ± 0.9 | 3.2 ± 0.9 | 7 ± 1 | 4.8 ± 0.6 |
| $[\mathbf{6}]NO_3$ | Ir/− | 5 ± 1 | 5 ± 1 | 9.0 ± 0.7 | 8 ± 2 |
| $[\mathbf{7}]NO_3$ | Ru/− | 2.1 ± 0.3 | 4 ± 1 | 6.4 ± 0.9 | 4.2 ± 0.7 |

[a]DNA metalation with 5 $\mu$M $[\mathbf{1}]NO_3$ and $[\mathbf{2}]NO_3$ for 24 h is given in parentheses.

slightly more cytotoxic than the respective ruthenium analogue ($[\mathbf{1}]^+/[\mathbf{3}]^+/[\mathbf{7}]^+$). Second, flurbiprofen/ethacrynic acid conjugates ($[\mathbf{1,2}]^+$) are more cytotoxic than their biotin/ethacrynic acid counterparts ($[\mathbf{3,4}]^+$), while the opposite behavior is observed for the bipyridine ligands ($\mathbf{L}^{EF}$ being substantially noncytotoxic while $\mathbf{L}^{EB}$ shows $IC_{50}$ values comparable to those of its complexes). Third, cancer cell selectivity (i.e., $IC_{50}$ found for nontumorigenic HEK293/$IC_{50}$ found for the cancer cell line) increases on going from $[\mathbf{3}]^+/[\mathbf{4}]^+$ to $[\mathbf{1}]^+/[\mathbf{2}]^+$, peaking at ca. 4 for $[\mathbf{2}]NO_3$ in A2780 cells. These trends hold for all of the tested cell lines, indicating that the cytotoxic effect of $[\mathbf{1-4}]^+$ is heavily influenced by the selection of metal center and bioactive fragments and evidencing iridium/ethacrynic acid/flurbiprofen as the best combination. Notably, ruthenium and iridium bipyridine with simple methyl esters on the bipyridine ligand ($[\mathbf{6}]^+/[\mathbf{7}]^+$) are considerably less cytotoxic than the bis-conjugated derivatives $[\mathbf{1-4}]^+$, suggesting that synergic effects are responsible for the biological activity of the latter. Note that incubation of a 1:1:1 mixture of flurbiprofen, ethacrynic acid, and the Ru/Ir complex lacking bioactive fragments ($[\mathbf{6}]^+$ and $[\mathbf{7}]^+$) resulted in a 5−12-fold lower cytotoxicity with respect to the administration of a single compound ($[\mathbf{1}]^+$ and $[\mathbf{2}]^+$). The overall better performance of flurbiprofen/ethacrynic acid derivatives $[\mathbf{1,2}]^+$, with respect to the biotin/ethacrynic acid analogues $[\mathbf{3,4}]^+$ may in part be related to a more controlled ester hydrolysis in the cellular environment (see above). It is noteworthy that biotinylated derivatives were not particularly effective also among the bis-functionalized platinum(IV) complexes (Scheme 1a).[4a−g]

In order to gain insights into the mode of action of the compounds, A2780 cells were incubated with 10 $\mu$M of $[\mathbf{1-7}]^+$ for 8 and 24 h and 5 $\mu$M of $[\mathbf{1-7}]^+$ for 24 h, and the metal content was determined by ICP-MS following established protocols (Table 3).[22] The cellular uptake for all tested compounds increases with incubation time and with concentration. Treatment with ethacrynic acid/flurbiprofen conjugates $[\mathbf{1,2}]^+$ resulted in a substantially higher metal accumulation with respect to the nonfunctionalized reference complexes $[\mathbf{6,7}]^+$. In contrast, biotin-functionalized complexes $[\mathbf{3,4}]^+$ showed only a modest increase in cellular internalization, and the ruthenium content determined for the bis-penicillin $[\mathbf{5}]^+$ and the bis-methyl $[\mathbf{7}]^+$ esters was not significantly different. The DNA metalation level, following incubation with 10 $\mu$M of $[\mathbf{1-7}]^+$ for 24 h, decreases in the sequence $[\mathbf{1}]^+ \gg [\mathbf{3}]^+ \approx [\mathbf{5}]^+ \approx [\mathbf{7}]^+$ and $[\mathbf{2}]^+ \gg [\mathbf{4}]^+ > [\mathbf{6}]^+$ for Ru and Ir complexes, respectively, reflecting the amount of compound taken up by the cells in an almost linear fashion (Figure S45). Overall, these data correlate well with A2780 cytotoxicity, which is the highest for compounds better internalized by the cells (i.e., $[\mathbf{1}]^+$ and $[\mathbf{2}]^+$).

To further explore whether DNA metalation plays a role in the cell-killing effect of the investigated compounds, we measured their antiproliferative activity in a pair of Chinese hamster ovary cell lines, CHO-K1 (wild-type) and its mutant cell line MMC-2. The latter is deficient in the DNA nucleotide excision repair (NER); thus, the DNA damage in MMC-2 cells is more harmful than in the NER-proficient CHO-K1 cells. The degree of DNA damage involvement in the mechanism of action can be estimated from the ratio of $IC_{50}$ values estimated for CHO-K1 and MMC-2 cells (factor $F$ in Table 4). The four

**Table 4. Antiproliferative Data ($IC_{50}/\mu M$)[a] for CHO-K1 (Wild-Type) and MMC-2 (NER-Deficient) Cells Treated with $[\mathbf{1-4}]NO_3$ and Cisplatin[b]**

| compound | CHO-K1 | MMC-2 | $F$[c] |
|---|---|---|---|
| $[\mathbf{1}]NO_3$ | 23 ± 4 | 12.9 ± 0.3 | 1.8 |
| $[\mathbf{2}]NO_3$ | 18.9 ± 0.6 | 10.1 ± 0.2 | 1.9 |
| $[\mathbf{3}]NO_3$ | 29 ± 2 | 9.1 ± 0.7 | 3.2 |
| $[\mathbf{4}]NO_3$ | 25.7 ± 0.8 | 8.9 ± 0.2 | 2.9 |
| cisplatin | 29 ± 1 | 3.3 ± 0.1 | 8.8 |

[a]Determined by MTT assay after 72 h treatment. [b]Values are given as mean ± SD. [c]Defined as $IC_{50}$(NER efficient)/$IC_{50}$(NER deficient).

Ru/Ir bioconjugated complexes $[\mathbf{1-4}]^+$ are slightly more efficient in the NER-deficient cell line MMC-2 than in the wild-type CHO-K1; this effect is more pronounced for the biotin derivatives $[\mathbf{3,4}]^+$ in comparison to the flurbiprofen derivatives $[\mathbf{1,2}]^+$ (Figure S46). The prominent involvement of DNA damage in cells treated with cisplatin is apparent, the compound being 9 times more active in the NER-deficient cells.

Next, we performed cell viability studies of $[\mathbf{1-4}]^+$ and cisplatin in A2780 cells using the MTT assay with variable treatment times (24/48/72 h; Table 5). The effect of DNA metalation resulting in DNA damage is usually related to the inhibition of DNA replication or transcription, which only becomes apparent after a longer time of the treatment (after at least one cell cycle is completed). Cisplatin is a typical example of this behavior, whose mechanism of action is primarily related to its ability to modify DNA, and its cytotoxicity is strongly time-dependent. Indeed, the $IC_{50}$ values obtained for cisplatin after 24 h were markedly higher (9 times) than those determined after 72 h treatment. Conversely, we observed almost no variation of the $IC_{50}$ values along the treatment times (except for $[\mathbf{3}]NO_3$ at 24 h). Thus, it seems reasonable to suggest that the cytotoxic effects of $[\mathbf{1-4}]^+$ might contribute


https://doi.org/10.1021/acs.inorgchem.1c00641
Inorg. Chem. 2021, 60, 9529−9541

**Table 5. Antiproliferative Data ($IC_{50}/\mu M$) for $[1-4]NO_3$ and Cisplatin in A2780 Cells with Variable Treatment Times**[a]

| | $IC_{50}$ ($\mu$M) | | |
|---|---|---|---|
| compound | 24 h | 48 h | 72 h |
| $[1]NO_3$ | 6.7 ± 0.2 | 6.1 ± 0.3 | 5.6 ± 0.3 |
| $[2]NO_3$ | 3.0 ± 0.1 | 2.9 ± 0.1 | 2.8 ± 0.1 |
| $[3]NO_3$ | 20 ± 2 | 12.7 ± 0.2 | 11.1 ± 0.4 |
| $[4]NO_3$ | 8 ± 1 | 7.6 ± 0.8 | 7.0 ± 0.8 |
| cisplatin | 34 ± 4 | 4.9 ± 0.9 | 3.6 ± 0.7 |

[a]Values are given as mean ± SD.

to the overall cell growth inhibition more than their antiproliferative effects. In accordance with the antiproliferative activity in cell lines proficient and deficient in NER (Table 4), these results support the view that DNA metalation might be involved in the mechanism of action of $[1-4]^+$, although other routes are likely to play a more significant role.

In this respect, we performed experiments to assess whether the ethacrynic acid/flurbiprofen derivatized complexes $[1,2]^+$ are able to affect glutathione *S*-transferase (GST) and cyclooxygenase (COX) activity.

Thus, lysates of the HeLa cells treated for 18 h with $[1]NO_3$ and $[2]NO_3$ at concentrations corresponding to their respective $IC_{50}$ values (determined with MTT after 72 h; Table 2) were prepared and analyzed with either Glutathione *S*-Transferase Fluorescent Activity Kit (Invitrogen) or Cyclooxygenase Activity Kit (Fluorimetric) (Abcam). Similarly, combinations of the nonfunctionalized complexes $[6]^+/[7]^+$ with the reference enzyme inhibitors (***F*-$CO_2H$/*E*-$CO_2H$**) or the bipyridine ligand $L^{EF}$ at identical concentrations were tested. The results are shown in Figure 1 and Figure S47. The GST activity was significantly reduced in the cells treated with both ethacrynic acid carrying compounds $[1]NO_3$ and $[2]NO_3$, as well as in the cells treated with the mixtures containing ***E*-$CO_2H$**. Nevertheless, $[1]NO_3$ and $[2]NO_3$ caused a stronger inhibition, reducing the enzyme activity to 68 and 62%, respectively. No significant inhibition of COX activity was observed, except for $[2]NO_3$.

In conclusion, the mechanism of action of the investigated compounds $[1-4]^+$ is likely multimodal, involving DNA metalation as well as enzyme inhibition. However, the cytotoxic effects associated with the enzyme inhibition activity possibly outweigh the effects caused by DNA metalation.

Enzyme inhibition by $[1]^+$ and $[2]^+$ could be enacted by metal-based species (e.g., the organometallic cations) or by the bioactive organic fragments that are released upon entering the cell. Judging from the stability studies in cell culture medium and the metal uptake experiments (*vide supra*), it is apparent that both the internalization of the compounds and the release of the bioactive groups from the respective Ir or Ru complexes are time-dependent. Nevertheless, the fact that cytotoxicity does not increase from 24 to 72 h (Table 5) points out that these compounds mostly exert their biological activity within the first 24 h of the treatment.

## CONCLUSIONS

Ruthenium(II) arene and iridium(III) cyclopentadienyl complexes are among the most investigated transition-metal compounds in the landscape of the development of new anticancer drugs able to overcome the limitations associated with the use of platinum chemotherapeutics. In addition, the conjugation with suitable bioactive fragments is an intriguing and well-established strategy aimed to improve the anticancer activity of a metal complex. Remarkably, the bis-functionalization of metal complexes with two different bioactive molecules appears to be an even more promising approach, which has been successfully investigated on platinum(IV) complexes, but its applicability to other metal structures remains undeveloped, possibly due to the lack of adequate synthetic routes. Here, we have employed a commercial bipyridine as a convenient starting material to obtain new half-sandwich Ru(II) and Ir(III) complexes doubly functionalized with different

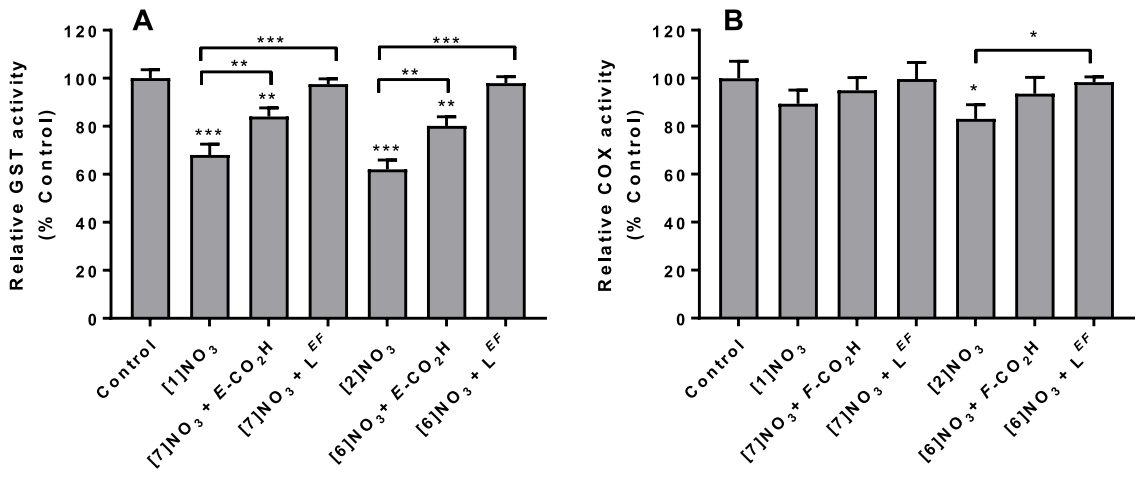


**Figure 1.** Effect of the tested compounds on GST (A) and COX (B) activity in HeLa cells. The cells were incubated with $[1]NO_3$ and $[2]NO_3$ at the concentrations corresponding to their respective $IC_{50}$ values (72 h; MTT) for 18 h. For comparison, the cells were also treated with combinations of $[7]NO_3$ and $[6]NO_3$ with ***E*-$CO_2H$** (A) and ***F*-$CO_2H$** (B) or with $L^{EF}$ at concentrations identical with those of $[1]NO_3$ or $[2]NO_3$, respectively. The enzyme activities are expressed in percent of enzyme activities in nontreated control cells. The GST activity was determined with Glutathione *S*-Transferase Fluorescent Activity Kit (Invitrogen). The COX activity was determined with Cyclooxygenase Activity Assay Kit (Fluorimetric) (Abcam). Statistical analysis was performed using Student's *t* test. Statistically significant differences from nontreated control are shown above the individual bars; statistically, significant differences between samples are given above the brackets (*$p \leq 0.05$; **$p \leq 0.01$, and ***$p \leq 0.001$).



https://doi.org/10.1021/acs.inorgchem.1c00641
Inorg. Chem. 2021, 60, 9529−9541

bioactive carboxylic acids, including heterofunctionalized derivatives. The complexes manifest a stable coordination environment and a variable tendency to release the bioactive molecules in aqueous media. Biological experiments on ovarian, breast, and cervical cancer cell lines revealed an improved cytotoxicity profile for both Ru(II) and Ir(III) complexes, with ethacrynic acid/flurbiprofen as the most effective combination. The activity of the compounds is associated with an increased cellular uptake, DNA metalation, and COX/GST enzyme inhibition. The last activity is possibly related to the bioactive carboxylic acids (or their derivatives) that are released by hydrolysis. Synergic effects on cytotoxicity and enzyme inhibition were clearly observed by control combination experiments. The efficacy of the proposed method strongly encourages further studies aimed at identifying other combinations of bioactive molecules and may be easily extended to other metal scaffolds investigated for pharmacological activity.

## EXPERIMENTAL SECTION

**General Experimental Details.** $RuCl_3{\cdot}xH_2O$ (41.9% Ru; Chimet S.p.A), $IrCl_3{\cdot}xH_2O$ (59.9% Ir; Merck), and other chemicals (≥99% purity) were purchased from Alfa Aesar, Merck, Apollo Scientific, or TCI Chemicals. Ethacrynic acid (***E*-CO$_2$H**),[23] flurbiprofen (***F*-CO$_2$H**),[23] biotin (***B*-CO$_2$H**),[23] potassium benzylpenicillin (K[***P*-CO$_2$**]),[23] 2,2′-bipyridine-4,4′-dicarboxylic acid, and ethyl-(diisopropylamino)carboxydiimide hydrochloride (EDCI·HCl; at −20 °C) were stored under $N_2$ as received. Ethylene glycol was dried under high vacuum over $P_2O_5$ and stored under $N_2$. Column chromatography was carried out with silica gel (70−230 mesh).

$[RuCl_2(\eta^6\text{-}p\text{-cymene})]_2$,[24] $[IrCl_2(\eta^5\text{-}C_5Me_5)]_2$,[25] and bipyridine ligands[5] $\mathbf{L}^{EF}$ and $\mathbf{L}^{EB}$ were synthesized according to literature methods. All operations were carried out in air with common laboratory glassware, except for the syntheses of the bioconjugated bipyridine ligands [**2**]Cl and [**4**]Cl, which were carried out under $N_2$ using standard Schlenk techniques and solvents distilled from appropriate drying agents (DMF from BaO, THF from $CaH_2$, $CH_2Cl_2$ and $CHCl_3$ from $P_2O_5$). Once isolated, organic bipyridine esters were stored at 4 °C; all Ru and Ir compounds were air- and moisture-stable in the solid state at room temperature. NMR spectra were recorded at 25 °C on a Bruker Avance II DRX400 instrument equipped with a BBFO broad-band probe. Chemical shifts (in ppm) are referenced to the residual solvent peaks[26] ($^1$H, $^{13}$C) or to external standards[27] ($^{14}$N to $CH_3NO_2$, $^{19}$F to $CFCl_3$, $^{35}$Cl to 1 M NaCl in $D_2O$). $^1$H and $^{13}$C spectra were assigned with the aid of $^{13}$C DEPT 135, $^1$H−$^1$H COSY, $^1$H−$^{13}$C *gs*-HSQC and $^1$H−$^{13}$C *gs*-HMBC experiments.[28] $CDCl_3$ for NMR analysis was stored in the dark over $Na_2CO_3$. IR spectra (650−4000 $cm^{-1}$) were recorded on a PerkinElmer Spectrum One FT-IR spectrometer, equipped with a UATR sampling accessory and processed with Spectragryph software.[29] CHNS analyses were performed on a Vario MICRO cube instrument (Elementar). ESI-Q/ToF flow injection analyses (FIA) were conducted on a 1200 Infinity HPLC coupled to a Jet Stream ESI interface with a 6530 Infinity Q-TOF quadrupole time of flight tandem mass spectrometer (Agilent Technologies, USA). HPLC-MS grade acetonitrile was used as the mobile phase (Carlo Erba, Italy). The flow rate was 0.2 mL/min (total run time 3 min), and the injection volume was 3 μL. ESI operating conditions: drying gas ($N_2$, purity >98%), 350 °C and 10 L/min; capillary voltage 4.5 kV; nozzle voltage 1 kV; nebulizer gas 35 psig; sheath gas ($N_2$, purity >98%) 375 °C and 11 L/min. The fragmentor was kept at 50 V, the skimmer at 65 V, and the OCT 1 RF at 750 V. High-resolution MS and MS/MS spectra were obtained in the positive mode in the range 100−1700 *m*/*z*; the mass axis was routinely calibrated using the tuning mix HP0321 (Agilent Technologies) prepared in acetonitrile and water. Prior to injection, each sample was properly diluted to ca. 20 μg/g. Analytical and spectroscopic and spectrometric characterizations of compounds are given in the Supporting Information.

**Synthesis of Compounds.** *Bis(2-chloroethyl)[2,2′-bipyridine]-4,4′-dicarboxylate (Chart 1).* In a 50 mL Schlenk tube under $N_2$,

**Chart 1. Structure of Bis(2-chloroethyl)[2,2′-bipyridine]-4,4′-dicarboxylate**

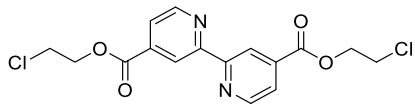


2,2′-bipyridine-4,4′-dicarboxylic acid (529 mg, 2.17 mmol), DMAP (65 mg, 0.57 mmol), EDCI·HCl (992 mg, 5.17 mmol), THF (12 mL), and 2-chloroethanol (0.30 mL, 4.47 mmol) were introduced in that order. The milky colorless suspension was stirred at room temperature overnight, affording a colorless solution and a pink solid. Volatiles were removed under vacuum; the residue was suspended in $CH_2Cl_2$ and moved on top of a silica column (height 4 cm, diameter 3.5 cm). Impurities were eluted with $CH_2Cl_2$ (40 mL), and the title compound was eluted with a $CH_2Cl_2$/hexane/acetone 10/5/2 v/v/v mixture (85 mL). Following removal of the volatiles under vacuum (40 °C), the resulting colorless solid was dried under vacuum (RT over $P_2O_5$) and then stored under $N_2$. Yield: 465 mg, 58%.

*Bis(2-benzylpenicillinyloxyethyl)[2,2′-bipyridine]-4,4′-dicarboxylate ($L^{PP}$) (Chart 2).* In a 50 mL Schlenk tube under $N_2$, bis(2-chloroethyl)[2,2′-bipyridine]-4,4′-dicarboxylate (202 mg, 0.546 mmol), K[***P*-CO$_2$**] (544 mg, 1.46 mmol), and DMF (8 mL) were introduced. The suspension (colorless solution + solid) was stirred at 85 °C for 18 h. The conversion was checked by $^1$H NMR ($CDCl_3$), and then the brown suspension was cooled to room temperature and volatiles were removed under vacuum. The residue was suspended in acetone and filtered over a short silica pad. The filtrate was taken to dryness under vacuum; the residue was dissolved in $CH_2Cl_2$ and moved on top of a silica column (height 6 cm, diameter 2.5 cm). Impurities were eluted with $CH_2Cl_2$, and the title compound was eluted with $CH_2Cl_2$/acetone (7/1 to 3/1 v/v gradient). Following removal of the volatiles under vacuum, the resulting pale yellow foamy solid was dried under vacuum (RT over $P_2O_5$) and then stored at 4 °C. Yield: 201 mg, 37%.

*Synthesis of Ru and Ir Compounds. Method A.* A solution of $[RuCl_2(\eta^6\text{-}p\text{-cymene})]_2$ or $[IrCl_2(\eta^5\text{-}C_5Me_5)]_2$ (20−50 mg) in MeCN (2 mL) was treated with $AgNO_3$ (2.0 equiv) and stirred at room temperature in the dark. After 1 h, the suspension (yellow/orange solution + colorless solid) was filtered over a Celite pad. The selected bipyridine ligand (2.0 equiv) was added to the filtrate, and the mixture was stirred at reflux for 1−2 h. Next, the conversion was checked by NMR ($^1$H $CDCl_3$) and the volatiles were removed under vacuum. The residue was dissolved in $CH_2Cl_2$ and the solution was filtered through Celite. The filtrate was dried under vacuum; the resulting ocher yellow (Ru) or orange (Ir) solid was washed with $Et_2O$ and dried under vacuum (40 °C).

*Method B.* In a 25 mL Schlenk tube, a solution of $[IrCl_2(\eta^5\text{-}C_5Me_5)]_2$ (ca. 25 mg) and the selected bipyridine (2.0 equiv) in $CHCl_3$ (8 mL) was stirred at reflux for 14 h. The resulting orange solution was taken to dryness under vacuum, and the residue was triturated in $Et_2O$. The suspension was filtered; the orange solid, namely $[IrCl(\eta^5\text{-}C_5Me_5)(\text{bipyridine})]Cl$, was washed with $Et_2O$ and dried under vacuum (40 °C). Subsequently, a fraction of the Ir compound (ca. 60 mg) was dissolved in MeCN (2 mL) and treated with $AgNO_3$ (1.0 equiv). The suspension was stirred at room temperature in the dark for 4 h. Next, the mixture (orange solution + colorless solid) was filtered over a Celite pad and the filtrate was taken to dryness under vacuum. The residue was dissolved in $CH_2Cl_2$ and filtered again through Celite. The filtrate was dried under vacuum; the resulting orange solid was washed with $Et_2O$ and dried under vacuum (40 °C).


https://doi.org/10.1021/acs.inorgchem.1c00641
Inorg. Chem. 2021, 60, 9529−9541

**Chart 2. Structure of $L^{PP}$**

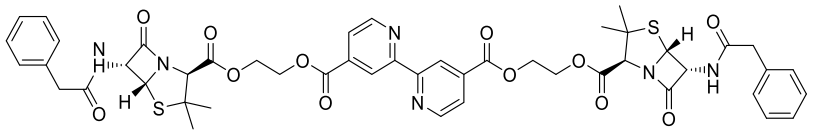

**Chart 3. Structure of $[1]^+$**

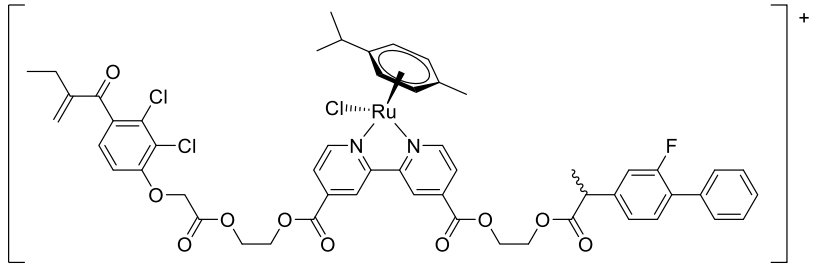

**Chart 4. Structure of $[2]^+$**

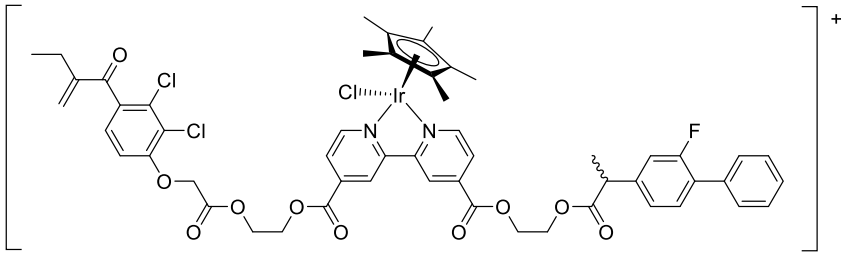

**Chart 5. Structure of $[3]^+$**

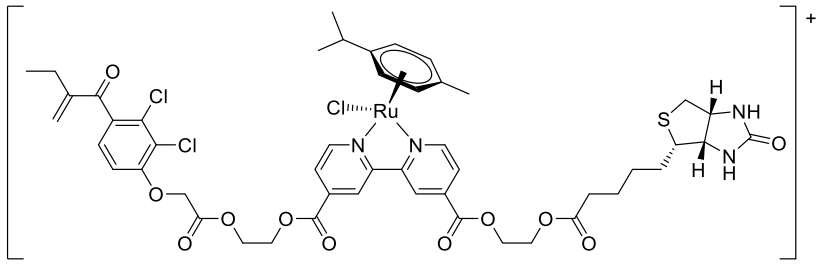

**Chart 6. Structure of $[4]^+$**

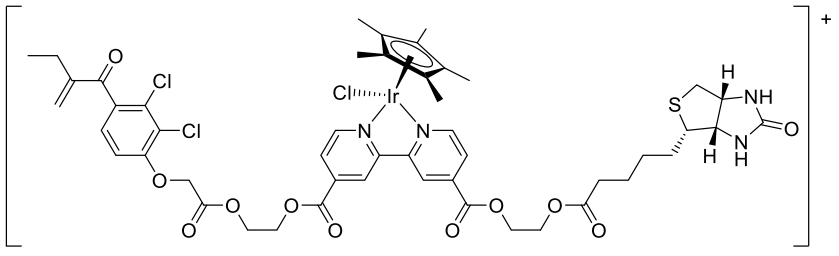

*Note*: the use of methanol as an alternative solvent for these procedure is NOT recommended, due to transesterification processes (*vide infra*).[30]

*[RuCl($\eta^6$-p-cymene)($\kappa^2$N-$L^{EF}$)]$NO_3$ ([1]$NO_3$) (Chart 3).* The complex was prepared using $[RuCl_2(\eta^6\text{-}p\text{-cymene})]_2$ (30 mg, 0.05 mmol), $AgNO_3$ (17 mg, 0.10 mmol) and $L^{EF}$ (86 mg, 0.10 mmol), according to method A. Yield: 102 mg, 88%.

*[IrCl($\eta^5$-$C_5Me_5$)($\kappa^2$N-$L^{EF}$)]$^+$ ([2]$^+$) (Chart 4).* [2]Cl was prepared using $[IrCl_2(\eta^5\text{-}C_5Me_5)]_2$ (26 mg, 0.033 mmol) and $L^{EF}$ (58 mg, 0.069 mmol), according to method B. Yield: 79 mg, 98%. [2]$NO_3$ was prepared using $[IrCl_2(\eta^5\text{-}C_5Me_5)]_2$ (35 mg, 0.045 mmol), $AgNO_3$ (15 mg, 0.088 mmol), and $L^{EF}$ (76 mg, 0.089 mmol), according to method A. Yield: 104 mg, 93%. An alternative preparation from [2]Cl (79 mg, 0.064 mmol) and $AgNO_3$ (11 mg, 0.064 mmol) followed method B. Yield: 67 mg, 83%.

*[RuCl($\eta^6$-p-cymene)($\kappa^2$N-$L^{EB}$)]$NO_3$ ([3]$NO_3$) (Chart 5).* The complex was prepared using $[RuCl_2(\eta^6\text{-}p\text{-cymene})]_2$ (30 mg, 0.05 mmol), $AgNO_3$ (17 mg, 0.10 mmol), and $L^{EB}$ (84 mg, 0.10 mmol), according to method A. Yield: 109 mg, 95%.

*[IrCl($\eta^5$-$C_5Me_5$)($\kappa^2$N-$L^{EB}$)]$^+$ ([4]$^+$) (Chart 6).* [4]Cl was prepared using $[IrCl_2(\eta^5\text{-}C_5Me_5)]_2$ (27 mg, 0.034 mmol), and $L^{EB}$ (58 mg, 0.067 mmol), according to method B. Yield: 78 mg, 94%. [4]$NO_3$ was



https://doi.org/10.1021/acs.inorgchem.1c00641
Inorg. Chem. 2021, 60, 9529−9541

**Chart 7. Structure of $[5]^+$**

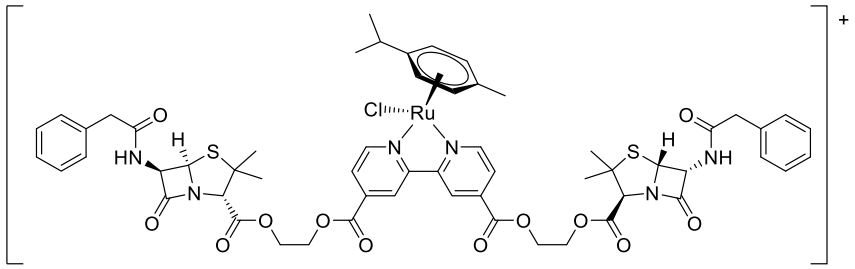

prepared using $[IrCl_2(\eta^5\text{-}C_5Me_5)]_2$ (36 mg, 0.045 mmol), $AgNO_3$ (16 mg, 0.091 mmol), and $\mathbf{L}^{EB}$ (77 mg, 0.091 mmol), according to method A. Yield: 110 mg, 95%. An alternative preparation from [**4**]Cl (60 mg, 0.048 mmol) and $AgNO_3$ (9 mg, 0.053 mmol) followed method B. Yield: 51 mg, 83%.

*[RuCl($\eta^6$-p-cymene)($\kappa^2$N-$\mathbf{L}^{PP}$)]$NO_3$ ([**5**]$NO_3$) (Chart 7).* The complex was prepared using $[RuCl_2(\eta^6\text{-}p\text{-cymene})]_2$ (17 mg, 0.028 mmol), $AgNO_3$ (10 mg, 0.059 mmol), and $\mathbf{L}^{PP}$ (55 mg, 0.057 mmol), according to method A. Yield: 68 mg, 94%.

*Dimethyl[2,2′-bipyridine]-4,4′-dicarboxylate ($\mathbf{L}^{MeMe}$) (Chart 8).* The title compound was prepared according to a modified literature

**Chart 8. Structure of $\mathbf{L}^{MeMe}$**

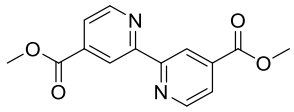

procedure.[16] In a 100 mL round-bottom flask, 98% $H_2SO_4$ (1.6 mL, 30 mmol) was added dropwise to a suspension of 2,2′-bipyridine-4,4′-dicarboxylic acid (502 mg, 2.06 mmol) in MeOH (30 mL). The mixture was stirred at reflux for 29 h. The resulting pink solution was cooled to room temperature, and NaOH (1 M in water, 30 mL, 30 mmol) was added dropwise. Subsequently, MeOH was removed under reduced pressure and the mixture (pink aqueous solution + colorless precipitate) was extracted with $CH_2Cl_2$ (3 × 40 mL). The combined organic extracts were filtered through a Celite pad and dried under vacuum. The resulting colorless solid was washed with $Et_2O$ and dried under vacuum (40 °C). Yield: 509 mg, 91%.

*[IrCl($\eta^5$-$C_5Me_5$)($\kappa^2$N-$\mathbf{L}^{MeMe}$)]X ([**6**]X; X = $NO_3$, $BF_4$) (Chart 9).* The synthesis of the related compound [**6**]Cl from $[IrCl_2(\eta^5\text{-}C_5Me_5)]_2$/

**Chart 9. Structure of $[6]^+$**

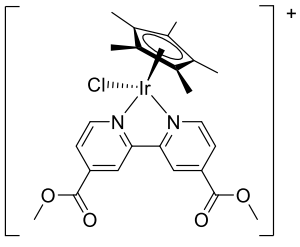

$\mathbf{L}^{MeMe}$ was previously reported.[18] [**6**]$NO_3$ was prepared using $[IrCl_2(\eta^5\text{-}C_5Me_5)]_2$ (36 mg, 0.069 mmol), $AgNO_3$ (24 mg, 0.14 mmol), and $\mathbf{L}^{MeMe}$ (38 mg, 0.14 mmol), according to method A. Yield: 85 mg, 83%. [**6**]$BF_4$ was prepared by dissolution of compound [**6**]$NO_3$ (51 mg, 0.073 mmol) in acetone (5 mL), and the solution was treated with $NaBF_4$ (11 mg, 0.10 mmol). The mixture was heated at reflux for 4 h and then taken to dryness under vacuum. The residue was suspended in $CH_2Cl_2$ and filtered through a Celite pad, in order to remove $NaNO_3$. The filtrate was taken to dryness under vacuum and dissolved in MeOH (ca. 3 mL). The solution was heated to reflux then cooled to room temperature. The resulting bright orange crystalline solid was collected by filtration, washed with $Et_2O$, and dried under vacuum (40 °C). Yield: 47 mg, 89%. X-ray-quality crystals of [**6**]$BF_4$ were obtained from a MeCN solution layered with $Et_2O$ and set aside at −20 °C (Table S1 and Figure S34).

*[RuCl($\eta^6$-p-cymene)($\kappa^2$N-$\mathbf{L}^{MeMe}$)]$NO_3$ ([**7**]$NO_3$) (Chart 10).* The complex was prepared using $[RuCl_2(\eta^6\text{-}p\text{-cymene})]_2$ (57 mg, 0.093 mmol), $AgNO_3$ (32 mg, 0.19 mmol), and $\mathbf{L}^{MeMe}$ (51 mg, 0.19 mmol), according to method A. Yield: 107 mg, 96%.

**Chart 10. Structure of $[7]^+$**

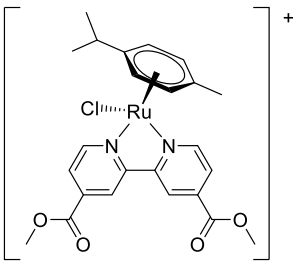

**X-ray Crystallography.** XRD experiments were performed using Mo K$\alpha$ radiation on a Bruker APEX II diffractometer equipped with a PHOTON2 detector. Data were corrected for Lorentz−polarization and absorption effects (empirical absorption correction SADABS).[31] The structure was solved by direct methods and refined by full-matrix least squares on the basis of all data using $F^2$.[32] H atoms were fixed at calculated positions and refined by a riding model. Non-hydrogen atoms were refined with anisotropic displacement parameters. Crystal data and collection details for [**6**]$BF_4$ are reported in Table S1.

**Solution Stability Studies.** *Stability in DMSO/Water.* The selected Ru or Ir compound ($1.0 \times 10^{-2}$ M for [**1**−**5**]$NO_3$; $2 \times 10^{-2}$ M for [**6**,**7**]$NO_3$) was dissolved in a DMSO-$d_6$/$D_2O$ 5/1 v/v solution (0.6 mL) containing dimethyl sulfone ($Me_2SO_2$, $5 \times 10^{-3}$ M) as an internal standard for $^1$H NMR[33] ($\delta$ 2.96 ppm (s, 6H) in DMSO-$d_6$/$D_2O$ 5/1). A single set of $^1$H and $^{19}$F{$^1$H} NMR signals was observed for the freshly prepared yellow (Ir) or orange (Ru) solution, attributed to the starting material. Next, the solution was heated to 37 °C for 72 h and NMR analyses were repeated (Figures S35−S41). The percent amount of starting material in solution with respect to the initial spectrum, falling in the 96−98% range for all compounds, was calculated by $^1$H NMR integration with respect to $Me_2SO_2$ as an internal standard. NMR data for the tested compounds are reported in the Supporting Information (DMSO-$d_6$/$D_2O$ 5/1 v/v solutions); chemical shifts are referenced to the residual peak as in pure DMSO-$d_6$ ($\delta$/ppm 2.50).

*Chloride/Solvent Exchange in DMSO/Water.* A DMSO-$d_6$/$D_2O$ 5/1 v/v solution of [**6**]$NO_3$ or [**7**]$NO_3$ (0.5 mL; $2 \times 10^{-2}$ M) was maintained at 37 °C for up to 86 h and then analyzed by $^{14}$N and $^{35}$Cl NMR (2000 scans).[34] Subsequently, $Ag(CF_3SO_3)$ was added (0.10 mL of a 0.12 M solution in DMSO-$d_6$/$D_2O$ 2/1 v/v; 1.2 equiv) and the NMR tube was kept in the dark at 50 °C for 5 h, affording an orange (Ru) or yellow (Ir) solution and a colorless precipitate (AgCl). The solid was separated, and $^1$H, $^{14}$N, and $^{19}$F{$^1$H} NMR spectra were recorded. Complete ([**6**]$^+$) or partial ([**7**]$^+$, ∼50%) conversion of the starting material was observed in the $^1$H NMR spectrum (Figures S40 and S41). The new set of signals, shifted to


https://doi.org/10.1021/acs.inorgchem.1c00641
Inorg. Chem. 2021, 60, 9529−9541

low field with respect to the starting metal chlorido species, was attributed to the solvato species $[Ir(\eta^5\text{-}C_5Me_5)(\mathbf{L}^{MeMe})(solv)]^{2+}$ ($[\mathbf{6}^{S}]^{2+}$) and $[Ru(\eta^6\text{-}p\text{-cymene})(\mathbf{L}^{MeMe})(solv)]^{2+}$ ($[\mathbf{7}^{S}]^{2+}$) (*solv* = $D_2O$, DMSO-$d_6$; Scheme S1). No solvolysis of metal−chloride bonds occurred before $Ag(CF_3SO_3)$ addition, as indicated by the absence of a $^{35}Cl$ NMR signal and comparison with $^1H$ NMR data for the solvato species $[\mathbf{6}^{S}]^{2+}$ and $[\mathbf{7}^{S}]^{2+}$.

*Stability in Methanol.* A freshly prepared solution of the selected compound in $CD_3OD$ (0.6 mL; $5 \times 10^{-3}$ M) was analyzed by $^1H$ and $^{19}F\{^1H\}$ NMR. Next the orange (Ru) or yellow/orange (Ir) solution was maintained at room temperature (~25 °C) and periodically analyzed by $^1H$ and $^{19}F\{^1H\}$ NMR. Once equilibrium was reached (no further change observed in NMR spectra), 1D and 2D NMR experiments ($^1H$, $^{13}C$, $^{19}F$, $^{14}N$, $^{13}C$-DEPT 135, $^1H-^1H$ COSY, $^1H-^{13}C$ *gs*-HSQC, $^1H-^{13}C$ *gs*-HMBC) were performed for a complete spectral assignment. The identity of compounds in solution (Schemes S2−S7) was checked by comparison with NMR data of the pure compounds and by ESI-MS(+) spectrometry on $CH_3OH$ solutions in the case of $[\mathbf{3}]^+$ and $[\mathbf{4}]^+$. The relative amount of compounds in solution (%) was calculated by $^1H$ NMR integration. Experimental details and MS and NMR data ($CH_3OH$ and $CD_3OD$, respectively) for the tested compounds are reported in Figures S42−S44 and Tables S2−S4 in the Supporting Information.

*Stability in Cell Culture Medium.* A stock solution of the selected Ru/Ir compound (ca. $3 \times 10^{-3}$ mmol/g) was prepared in DMSO and stored at room temperature. An RPMI 1640 cell culture medium (Sigma-Aldrich) was treated with $NaH_2PO_4/Na_2HPO_4$ ($c_{PO_4}$ = 190 mM, pH 7.35) and then stored at 4 °C under $N_2$. In three 2 mL vials, the stock solution (20 μL) was added to the cell culture medium (2.0 mL) and the final mixtures (Ru/Ir ca. 45 μmol/g, 1% DMSO) were heated at 37 °C for different times (0/24/48 h) with stirring. A fourth reference solution was prepared by adding the stock solution (20 μL) to HPLC water (2.0 mL). Next, the solutions were filtered on PTFE syringe filters (0.45 μm) and analyzed by HPLC/ESI(+)-MS. LC separation was conducted on an analytical reversed-phase Poroshell 120 EC-C18 column (3.0 × 75 mm, particle size 2.7 μm; Agilent Technologies) with a Zorbax precolumn (4.6 × 12.5 mm, particle size 5 μm; Agilent Technologies) at 30 °C. The separation was achieved using a gradient of formic acid (FA) 0.1% v/v in $H_2O$ (eluent A) and FA 0.1% v/v in $CH_3CN$ (eluent B), both LC-MS grade; the flow rate was 0.4 mL/min, and the injection volume was 4 μL. The elution program started from 95% A, hold for 2.6 min, then a linear gradient to 50% B in 13 min, then to 70% B in 5 min, and then to 100% B in 6 min, held for 5 min. Re-equilibration took 5 min. ESI operating conditions: drying gas ($N_2$, purity >98%) 350 °C and 10 L/min; capillary voltage 4.5 kV; nozzle voltage 1 kV; nebulizer gas 35 psig; sheath gas ($N_2$, purity >98%) 375 °C and 11 L/min. The fragmentor was at 175 V, the skimmer at 65 V, and the OCT 1 RF at 750 V. High-resolution MS spectra were achieved from 5 to 30 min in positive mode in the range 100−1700 *m*/*z*; the mass axis was calibrated daily using the Agilent tuning mix HP0321 (Agilent Technologies) prepared in acetonitrile and water. Calibration curves for ***E*-$CO_2$H**, ***B*-$CO_2$H**, and ***F*-$CO_2$H** were derived in the 0.4−10 μM range from stock solutions containing the three analytes ca. 80 μmol/g in water, appropriately diluted in HPLC-grade water.

**Biological Studies.** *Cytotoxicity.* Human cell lines A2780 and A2780cisR (ovarian carcinoma) were obtained from the European Collection of Cell Cultures, HEK-293 (embryonic kidney) was obtained from the ATCC (Merck, Buchs, Switzerland), and MCF-7 (breast carcinoma) and HeLa (cervical carcinoma) were obtained from the ECACC (European Collection of Authenticated Cell Cultures, Salisbury). HEK-293T cells were provided by the biological screening facility (EPFL, Switzerland). CHO-K1 and MMC-2 (derived from CHO-K1) Chinese hamster ovary cell lines were provided by Miroslav Pirsel (Institute of Experimental Oncology SAS, Bratislava). Cell culture media RPMI 1640 GlutaMAX and DMEM GlutaMAX and penicillin/streptomycin were purchased from Life Technologies, and fetal bovine serum (FBS) was obtained from Merck. Cancer cells were cultured in RPMI 1640 GlutaMAX;HEK-293 and HEK-293T cells were cultured in DMEM GlutaMAX. Both media were supplemented with 10% FBS and 1% penicillin/streptomycin. The cells were cultured at 37 °C with $CO_2$ (5%). The resistance in A2780cisR cells was maintained by routine additions of cisplatin (2 μM) to the medium. The cytotoxicity was determined using the MTT assay.[35] Cells were seeded in flat-bottomed 96-well plates as suspensions in a prepared medium at a density of 4300 cells/well in 100 μL. Stock solutions of metal complexes were prepared in DMSO and sequentially diluted in the medium up to the desired concentration (0−200 μM range) and 0.5% DMSO. The cytotoxic effects of RAPTA-C and cisplatin were also assessed as negative and positive control experiments. The compounds were added to the cells following a 24 h preincubation in 100 μL aliquots, and the plates were incubated for an additional 72 h. MTT (20 μL, 5 mg/mL in Dulbecco's phosphate buffered saline) was then added to the cells, and the plates were incubated for another 4 h. The medium was removed, and the purple formazan products, formed by the mitochondrial dehydrogenase activity of vital cells, were dissolved in DMSO (100 μL/well). The absorbance directly proportional to the number of surviving cells was read at 590 nm using a SpectroMax M5e multimode microplate reader (using SoftMax Pro software, version 6.2.2). The percentage of surviving cells in treated wells vs untreated control wells was calculated; the resulting $IC_{50}$ values are reported as means ± standard deviation from two independent experiments, each comprising four tests per concentration level.

*Cellular Uptake.* A2780 cells were seeded at a density of $2 \times 10^6$ cells/Petri dish and incubated overnight. The cells were treated with the tested compounds at the concentrations and times given in the respective table. Following the treatment, the cells were harvested (trypsin), washed, and pelleted. The pellets were digested with HCl using a microwave digestion system (CEM Mars). The Ru/Ir amount was determined with ICP-MS.

*DNA Metalation.* After the treatment (see above), the cells were lyzed using DNAzol (DNAzol, MRC) reagent, following the manufacturer's protocol. The DNA content was determined spectrophotometrically; the samples were lyzed in 30% HCl (Suprapur, Merck Millipore), and the Ru/Ir content was quantified by ICP-MS.

*Enzyme Inhibition Assays. Preparation of Cell Lysates for Analysis of Enzyme Activities.* HeLa cells were seeded at a density of $3 \times 10^5$ cells/dish and incubated at 37 °C. The next day, the cells were treated with the investigated compounds or mixtures of their respective components at concentrations corresponding to the $IC_{50}$ values previously determined with MTT assays after 72 h. Following a further 18 h treatment, the cells were scraped, washed with PBS, and counted. Identical cell counts were pelleted and lyzed in PBS-based lysis buffer (1% NP40, 1 mM PMSF, cocktail of protease inhibitors) on ice for 15 min. The supernatant was cleared and immediately subjected to an enzyme activity analysis.

*Analysis of Glutathione S-Transferase activity.* The enzyme activity was evaluated with a Glutathione *S*-Transferase Fluorescent Activity Kit (Invitrogen) following the manufacturer's protocol. Briefly, the cell lysates were plated in several dilutions in the Assay Buffer. Master mix containing Detection Reagent and Glutathione was added to the wells. The fluorescence was read in a kinetic mode at 460 nm with excitation at 390 nm. After blank subtraction, the data were plotted as ΔRFU in the initial 5 min of the reaction. Data from three to five measurements were normalized to the data of nontreated control cells.

*Analysis of Cyclooxygenase (COX) Activity.* The enzyme activity was evaluated with a Cyclooxygenase Activity Assay Kit (Abcam) following the manufacturer's protocol. Briefly, the cell lysates were plated in several dilutions in Assay Buffer. Then the Reaction Mix containing COX Probe and COX Cofactor was added to each well. The reaction was initiated with the addition of an arachidonic acid/NaOH solution. Fluorescence data were read in a kinetic mode at 587 nm with excitation at 535 nm. After blank subtraction, the data were plotted as ΔRFU in the initial 5 min of the reaction. Data from three to five measurements were normalized to the data of nontreated control cells.


https://doi.org/10.1021/acs.inorgchem.1c00641
Inorg. Chem. 2021, 60, 9529−9541

## ■ ASSOCIATED CONTENT

### Supporting Information

The Supporting Information is available free of charge at https://pubs.acs.org/doi/10.1021/acs.inorgchem.1c00641.

Characterization of compounds, including IR, NMR and MS spectra, X-ray diffraction data, and solution stability studies (NMR data). Additional biological data (cytotoxicity, enzyme inhibition assays) (PDF)

### Accession Codes

CCDC 2063385 contains the supplementary crystallographic data for this paper. These data can be obtained free of charge via www.ccdc.cam.ac.uk/data_request/cif, or by emailing data_request@ccdc.cam.ac.uk, or by contacting The Cambridge Crystallographic Data Centre, 12 Union Road, Cambridge CB2 1EZ, UK; fax: +44 1223 336033.

## ■ AUTHOR INFORMATION


### Corresponding Authors

**Lorenzo Biancalana** − *Dipartimento di Chimica e Chimica Industriale, Università di Pisa, I-56124 Pisa, Italy;* orcid.org/0000-0002-9276-0095; Email: lorenzo.biancalana@unipi.it

**Viktor Brabec** − *Czech Academy of Sciences, Institute of Biophysics, CZ-61265 Brno, Czech Republic;* orcid.org/0000-0002-8233-1393; Email: brabec@ibp.cz

### Authors

**Hana Kostrhunova** − *Czech Academy of Sciences, Institute of Biophysics, CZ-61265 Brno, Czech Republic*

**Lucinda K. Batchelor** − *Institut des Sciences et Ingénierie Chimiques, Ecole Polytechnique Fédérale de Lausanne (EPFL), CH-1015 Lausanne, Switzerland*

**Mouna Hadiji** − *Institut des Sciences et Ingénierie Chimiques, Ecole Polytechnique Fédérale de Lausanne (EPFL), CH-1015 Lausanne, Switzerland*

**Ilaria Degano** − *Dipartimento di Chimica e Chimica Industriale, Università di Pisa, I-56124 Pisa, Italy;* orcid.org/0000-0002-3585-8555

**Guido Pampaloni** − *Dipartimento di Chimica e Chimica Industriale, Università di Pisa, I-56124 Pisa, Italy*

**Stefano Zacchini** − *Dipartimento di Chimica Industriale "Toso Montanari", Università di Bologna, I-40136 Bologna, Italy;* orcid.org/0000-0003-0739-0518

**Paul J. Dyson** − *Institut des Sciences et Ingénierie Chimiques, Ecole Polytechnique Fédérale de Lausanne (EPFL), CH-1015 Lausanne, Switzerland;* orcid.org/0000-0003-3117-3249

**Fabio Marchetti** − *Dipartimento di Chimica e Chimica Industriale, Università di Pisa, I-56124 Pisa, Italy;* orcid.org/0000-0002-3683-8708

Complete contact information is available at: https://pubs.acs.org/10.1021/acs.inorgchem.1c00641


### Notes

The authors declare no competing financial interest.

## ■ ACKNOWLEDGMENTS

We gratefully thank the University of Pisa (Fondi di Ateneo 2020 and PRA_2020_39), the Czech Science Foundation (Grant 20-14082J), and the Swiss National Science Foundation for financial support.

## ■ REFERENCES


(1) (a) Štarha, P.; Trávníček, Z. Non-platinum complexes containing releasable biologically active ligands. *Coord. Chem. Rev.* **2019**, *395*, 130−145. (b) Kenny, R. G.; Marmion, C. J. Toward Multi-Targeted Platinum and Ruthenium Drugs-A New Paradigm in Cancer Drug Treatment Regimens? *Chem. Rev.* **2019**, *119*, 1058−1137. (c) Khoury, A.; Deo, K. M.; Aldrich-Wright, J. R. Recent advances in platinum-based chemotherapeutics that exhibit inhibitory and targeted mechanisms of action. *J. Inorg. Biochem.* **2020**, *207*, 111070. (d) Boros, E.; Dyson, P. J.; Gasser, G. Classification of Metal-based Drugs According to Their Mechanisms of Action. *Chem.* **2020**, *6*, 41−60.

(2) Selected references: (a) Ang, W. H.; Khalaila, I.; Allardyce, C. S.; Juillerat-Jeanneret, L.; Dyson, P. J. Rational design of platinum(IV) compounds to overcome glutathione-S-transferase mediated drug resistance. *J. Am. Chem. Soc.* **2005**, *127*, 1382−1383. (b) Cheng, Q.; Shi, H.; Wang, H.; Wang, J.; Liu, Y. Asplatin enhances drug efficacy by altering the cellular response. *Metallomics* **2016**, *8*, 672−678. (c) Nazarov, A. A.; Meier, S. M.; Zava, O.; Nosova, Y. N.; Milaeva, E. R.; Hartinger, C. G.; Dyson, P. J. Protein ruthenation and DNA alkylation: chlorambucil-functionalized RAPTA complexes and their anticancer activity. *Dalton Trans.* **2015**, *44*, 3614−3623. (d) Yang, J.; Sun, X.; Mao, W.; Sui, M.; Tang, J.; Shen, Y. Conjugate of Pt(IV)−Histone Deacetylase Inhibitor as a Prodrug for Cancer Chemotherapy. *Mol. Pharmaceutics* **2012**, *9*, 2793−2800. (e) Dhar, S.; Lippard, S. J. Mitaplatin, a potent fusion of cisplatin and the orphan drug dichloroacetate. *Proc. Natl. Acad. Sci. U. S. A.* **2009**, *106*, 22199−22204. (f) Petruzzella, E.; Phillip Braude, J.; Aldrich-Wright, J. R.; Gandin, V.; Gibson, D. A Quadruple-Action Platinum(IV) Prodrug with Anticancer Activity Against KRAS Mutated Cancer Cell Lines. *Angew. Chem., Int. Ed.* **2017**, *56*, 11539−11544.

(3) Gibson, D. Platinum(IV) anticancer agents; are we en route to the holy grail or to a dead end? *J. Inorg. Biochem.* **2021**, *217*, 111353.

(4) (a) Hu, W.; Fang, L.; Hua, W.; Gou, S. Biotin-Pt (IV)-indomethacin hybrid: A targeting anticancer prodrug providing enhanced cancer cellular uptake and reversing cisplatin resistance. *J. Inorg. Biochem.* **2017**, *175*, 47−57. (b) Petruzzella, E.; Sirota, R.; Solazzo, I.; Gandin, V.; Gibson, D. Triple action Pt(IV) derivatives of cisplatin: a new class of potent anticancer agents that overcome resistance. *Chem. Sci.* **2018**, *9*, 4299. (c) Babak, M. V.; Zhi, Y.; Czarny, B.; Boon Toh, T.; Hooi, L.; Kai-Hua Chow, E.; Ang, W. H.; Gibson, D.; Pastorin, G. Dual-Targeting Dual-Action Platinum(IV) Platform for Enhanced Anticancer Activity and Reduced Nephrotoxicity. *Angew. Chem., Int. Ed.* **2019**, *58*, 8109−8114. (d) Karmakar, S.; Poetsch, C.; Kowol, R.; Heffeter, P.; Gibson, D. Synthesis and Cytotoxicity of Water-Soluble Dual- and Triple-Action Satraplatin Derivatives: Replacement of Equatorial Chlorides of Satraplatin by Acetates. *Inorg. Chem.* **2019**, *58*, 16676−16688. (e) Shi, H.; Imberti, C.; Huang, H.; Hands-Portman, I.; Sadler, P. J. Biotinylated photoactive Pt(IV) anticancer complexes. *Chem. Commun.* **2020**, *56*, 2320−2323. (f) Babu, T.; Sarkar, A.; Karmakar, S.; Schmidt, C.; Gibson, D. Multiaction Pt(IV) Carbamate Complexes Can Codeliver Pt(II) Drugs and Amine Containing Bioactive Molecules. *Inorg. Chem.* **2020**, *59*, 5182−5193. (g) Muhammad, N.; Tan, C.-P.; Nawaz, U.; Wang, J.; Wang, F.-X.; Nasreen, S.; Ji, L.-N.; Mao, Z.-W. Multiaction Platinum(IV) Prodrug Containing Thymidylate Synthase Inhibitor and Metabolic Modifier against Triple-Negative Breast Cancer. *Inorg. Chem.* **2020**, *59*, 12632−12642. (h) Karmakar, S.; Kostrhunova, H.; Ctvrtlikova, T.; Novohradsky, V.; Gibson, D.; Brabec, V. Platinum(IV)-Estramustine Multiaction Prodrugs Are Effective Antiproliferative Agents against Prostate Cancer Cells. *J. Med. Chem.* **2020**, *63*, 13861−13877.

(5) Biancalana, L.; Batchelor, L. K.; Pereira, S. A. P.; Tseng, P.-J.; Zacchini, S.; Pampaloni, G.; Saraiva, L. M. F. S.; Dyson, P. J.; Marchetti, F. Bis-conjugation of Bioactive Molecules to Cisplatin-like Complexes through (2,2′-Bipyridine)-4,4′-Dicarboxylic Acid with Optimal Cytotoxicity Profile Provided by the Combination Ethacrynic Acid/Flurbiprofen. *Chem. - Eur. J.* **2020**, *26*, 17525−17535.

(6) (a) Nazarov, A. A.; Hartinger, C. G.; Dyson, P. J. Opening the lid on piano-stool complexes: an account of ruthenium (II)−arene complexes with medicinal applications. *J. Organomet. Chem.* **2014**, *751*, 251−260. (b) Murray, B. S.; Babak, M. V.; Hartinger, C. G.; Dyson, P. J. The development of RAPTA compounds for the treatment of tumors. *Coord. Chem. Rev.* **2016**, *306*, 86−114. (c) Anthony, E. J.; Bolitho, E. M.; Bridgewater, H. E.; Carter, O. W. L.; Donnelly, J. M.; Imberti, C.; Lant, E. C.; Lermyte, F.; Needham, R. J.; Palau, M.; Sadler, P. J.; Shi, H.; Wang, F.-X.; Zhang, W.-Y.; Zhang, Z. Metallodrugs are unique: opportunities and challenges of discovery and development. *Chem. Sci.* **2020**, *11*, 12888−12917. (d) Meier-Menches, S. M.; Gerner, C.; Berger, W.; Hartinger, C. G.; Keppler, B. K. Structure−activity relationships for ruthenium and osmium anticancer agents − towards clinical development. *Chem. Soc. Rev.* **2018**, *47*, 909−928. (e) Soldevila-Barreda, J. J.; Metzler-Nolte, N. Intracellular Catalysis with Selected Metal Complexes and Metallic Nanoparticles: Advances toward the Development of Catalytic Metallodrugs. *Chem. Rev.* **2019**, *119*, 829−869.

(7) (a) Movassaghi, S.; Leung, E.; Hanif, M.; Lee, B. Y. T.; Holtkamp, H. U.; Tu, J. K. Y.; Söhnel, T.; Jamieson, S. M. F.; Hartinger, C. G. A Bioactive L-Phenylalanine-Derived Arene in Multitargeted Organoruthenium Compounds: Impact on the Antiproliferative Activity and Mode of Action. *Inorg. Chem.* **2018**, *57*, 8521−8529. (b) Biancalana, L.; Gruchała, M.; Batchelor, L. K.; Błauż, A.; Monti, A.; Pampaloni, G.; Rychlik, B.; Dyson, P. J.; Marchetti, F. Conjugating Biotin to Ruthenium(II) Arene Units via Phosphine Ligand Functionalization. *Eur. J. Inorg. Chem.* **2020**, *2020*, 1061−1072.

(8) (a) Hayes, J. D.; Flanagan, J. U.; Jowsey, I. R. Glutathione transferases. *Annu. Rev. Pharmacol. Toxicol.* **2005**, *45*, 51−88. (b) Townsend, D. M.; Findlay, V. L.; Tew, K. D. Glutathione S-Transferases as Regulators of Kinase Pathways and Anticancer Drug Targets. *Methods Enzymol.* **2005**, *401*, 287−307.

(9) (a) Ang, W. H.; Parker, L. J.; De Luca, A.; Juillerat-Jeanneret, L.; Morton, C. J.; Lo Bello, M.; Parker, M. W.; Dyson, P. J. Rational design of an organometallic glutathione transferase inhibitor. *Angew. Chem., Int. Ed.* **2009**, *48*, 3854−3857. (b) Agonigi, G.; Riedel, T.; Zacchini, S.; Paunescu, E.; Pampaloni, G.; Bartalucci, N.; Dyson, P. J.; Marchetti, F. Synthesis and Antiproliferative Activity of New Ruthenium Complexes with Ethacrynic Acid-Modified Pyridine- and Triphenylphosphine-Ligands. *Inorg. Chem.* **2015**, *54*, 6504−6512. (c) Păunescu, E.; Soudani, M.; Martin, P.; Scopelliti, R.; Lo Bello, M.; Dyson, P. J. Organometallic Glutathione S-Transferase Inhibitors. *Organometallics* **2017**, *36*, 3313−3321.

(10) (a) Knights, K. M.; Mangoni, A. A.; Miners, J. O. Defining the COX inhibitor selectivity of NSAIDs: implications for understanding toxicity. *Expert Rev. Clin. Pharmacol.* **2010**, *3*, 769−776. (b) Regulski, M.; Regulska, K.; Prukała, W.; Piotrowska, H.; Stanisz, B.; Murias, M. COX-2 inhibitors: a novel strategy in the management of breast cancer. *Drug Discovery Today* **2016**, *21*, 598−615. (c) Tan, J.; Li, C.; Wang, Q.; Li, S.; Chen, S.; Zhang, J.; Wang, P. C.; Ren, L.; Liang, X.-J. A Carrier-Free Nanostructure Based on Platinum(IV) Prodrug Enhances Cellular Uptake and Cytotoxicity. *Mol. Pharmaceutics* **2018**, *15*, 1724−1728.

(11) (a) Raja, M. U.; Tauchman, J.; Therrien, B.; Süss-Fink, G.; Riedel, T.; Dyson, P. J. Arene ruthenium and pentamethylcyclopentadienyl rhodium and iridium complexes containing N,O-chelating ligands derived from piroxicam: Synthesis, molecular structure and cytotoxicity. *Inorg. Chim. Acta* **2014**, *409*, 479−483. (b) Paunescu, E.; McArthur, S.; Soudani, M.; Scopelliti, R.; Dyson, P. J. Nonsteroidal Anti-inflammatory Organometallic Anticancer Compounds. *Inorg. Chem.* **2016**, *55*, 1788−1808. (c) Biancalana, L.; Batchelor, L. K.; De Palo, A.; Zacchini, S.; Pampaloni, G.; Dyson, P. J.; Marchetti, F. A general strategy to add diversity to ruthenium arene complexes with bioactive organic compounds via a coordinated (4-hydroxyphenyl)-diphenylphosphine ligand. *Dalton Trans.* **2017**, *46*, 12001−12004. (d) Ashraf, A.; Aman, F.; Movassaghi, S.; Zafar, A.; Kubanik, M.; Siddiqui, W. A.; Reynisson, J. H.; Söhnel, T.; Jamieson, S. M.; Hanif, M. Structural Modifications of the Antiinflammatory Oxicam Scaffold and Preparation of Anticancer Organometallic Compounds. *Organometallics* **2019**, *38*, 361−374.

(12) (a) Maiti, S.; Paira, P. Biotin conjugated organic molecules and proteins for cancer therapy: A review. *Eur. J. Med. Chem.* **2018**, *145*, 206−223. (b) Bertrand, B.; O'Connell, M. A.; Waller, Z. A. E.; Bochmann, M. A Gold(III) Pincer Ligand Scaffold for the Synthesis of Binuclear and Bioconjugated Complexes: Synthesis and Anticancer Potential. *Chem. - Eur. J.* **2018**, *24*, 3613−3622. (c) Côrte-Real, L.; Karas, B.; Bras, A. R.; Pilon, A.; Avecilla, F.; Marques, F.; Preto, A.; Buckley, B. T.; Cooper, K. R.; Doherty, C.; Garcia, M. H.; Valente, A. Ruthenium−Cyclopentadienyl Bipyridine−Biotin Based Compounds: Synthesis and Biological Effect. *Inorg. Chem.* **2019**, *58*, 9135−9149. (d) Plazuk, D.; Zakrzewski, J.; Salmain, M.; Błauz, A.; Rychlik, B.; Strzelczyk, P.Ł; Bujacz, A.; Bujacz, G. Ferrocene−Biotin Conjugates Targeting Cancer Cells: Synthesis, Interaction with Avidin, Cytotoxic Properties and the Crystal Structure of the Complex of Avidin with a Biotin−Linker−Ferrocene Conjugate. *Organometallics* **2013**, *32*, 5774−5783.

(13) (a) Wu, S.; Zhou, Y.; Rebelein, J. G.; Kuhn, M.; Mallin, H.; Zhao, J.; Igareta, N. V.; Ward, T. R. Breaking Symmetry: Engineering Single-Chain Dimeric Streptavidin as Host for Artificial Metalloenzymes. *J. Am. Chem. Soc.* **2019**, *141*, 15869−15878. (b) Okamoto, Y.; Köhler, V.; Paul, C. E.; Hollmann, F.; Ward, T. R. Efficient In Situ Regeneration of NADH Mimics by an Artificial Metalloenzyme. *ACS Catal.* **2016**, *6*, 3553−3557. (c) Muñoz Robles, V.; Dürrenberger, M.; Heinisch, T.; Lledós, A.; Schirmer, T.; Ward, T. R.; Maréchal, J.-D. Structural, Kinetic, and Docking Studies of Artificial Imine Reductases Based on Biotin−Streptavidin Technology: An Induced Lock-and-Key Hypothesis. *J. Am. Chem. Soc.* **2014**, *136*, 15676−15683.

(14) (a) Lewandowski, E. M.; Skiba, J.; Torelli, N. J.; Rajnisz, A.; Solecka, J.; Kowalski, K.; Chen, Y. Antibacterial properties and atomic resolution X-ray complex crystal structure of a ruthenocene conjugated $\beta$-lactam antibiotic. *Chem. Commun.* **2015**, *51*, 6186−6189. (b) Skiba, J.; Rajnisz, A.; Navakoski de Oliveira, K.; Ott, I.; Solecka, J.; Kowalski, K. Ferrocenyl bioconjugates of ampicillin and 6-aminopenicillinic acid–synthesis, electrochemistry and biological activity. *Eur. J. Med. Chem.* **2012**, *57*, 234−239. (c) Ketikidis, J.; Banti, C. N.; Kourkoumelis, N.; Tsiafoulis, C. G.; Papachristodoulou, C.; Kalampounias, A. G.; Hadjikakou, S. K. Conjugation of Penicillin-G with Silver(I) Ions Expands Its Antimicrobial Activity against Gram Negative Bacteria. *Antibiotics* **2020**, *9*, 25.

(15) (a) Wheate, N. J.; Walker, S.; Craig, G. E.; Oun, R. The status of platinum anticancer drugs in the clinic and in clinical trials. *Dalton Trans.* **2010**, *39*, 8113−8127. (b) Yu, C.; Wang, Z.; Sun, Z.; Zhang, L.; Zhang, W.; Xu, Y.; Zhang, J.-J. Platinum-Based Combination Therapy: Molecular Rationale, Current Clinical Uses, and Future Perspectives. *J. Med. Chem.* **2020**, *63*, 13397−13412.

(16) (a) Zhang, D.; Dufek, E. J.; Clennan, E. L. Syntheses, Characterizations, and Properties of Electronically Perturbed 1,1′-Dimethyl-2,2′-bipyridinium Tetrafluoroborates. *J. Org. Chem.* **2006**, *71*, 315−319. (b) Miyoshi, D.; Karimata, H.; Wang, Z.-M.; Koumoto, K.; Sugimoto, N. Artificial G-Wire Switch with 2,2′-Bipyridine Units Responsive to Divalent Metal Ions. *J. Am. Chem. Soc.* **2007**, *129*, 5919−5925.

(17) To the best of our knowledge, only a few transition-metal benzylpenicillin complexes have been reported in the literature: (a) Grochowski, T.; Samochoka, K. Structural Characterization of the Platinum(II)-Penicillin Complexes. *Polyhedron* **1991**, *10*, 1473−1477. Refat, M. S.; Al-Saif, F. A. Spectroscopic and thermal investigations of transition and non-transition metal complexes of penicillin G as potential biological active species. *Russ. J. Gen. Chem.* **2014**, *84*, 143−156 (characterization limited to IR spectroscopy and magnetic analysis).

(18) The cation $[\mathbf{6}]^+$ was previously reported as a chloride salt: Brewster, T. P.; Miller, A. J. M.; Heinekey, D. M.; Goldberg, K. I. Hydrogenation of Carboxylic Acids Catalyzed by Half-Sandwich Complexes of Iridium and Rhodium. *J. Am. Chem. Soc.* **2013**, *135*, 16022−16025.



https://doi.org/10.1021/acs.inorgchem.1c00641
*Inorg. Chem.* 2021, 60, 9529−9541

(19) The maximum amount of water in these experiments—and thus the DMSO/water ratio—is limited by the solubility of the compounds and the millimolar concentration required for a good-quality $^{1}$H NMR spectrum.
(20) (a) Bugarcic, T.; Habtemariam, A.; Stepankova, J.; Heringova, P.; Kasparkova, J.; Deeth, R. J.; Johnstone, R. D. L.; Prescimone, A.; Parkin, A.; Parsons, S.; Brabec, V.; Sadler, P. J. The Contrasting Chemistry and Cancer Cell Cytotoxicity of Bipyridine and Bipyridinediol Ruthenium(II) Arene Complexes. *Inorg. Chem.* **2008**, *47*, 11470−11486. (b) Liu, Z.; Habtemariam, A.; Pizarro, A. M.; Fletcher, S. A.; Kisova, A.; Vrana, O.; Salassa, L.; Bruijnincx, P. C. A.; Clarkson, G. J.; Brabec, V.; Sadler, P. J. Organometallic Half-Sandwich Iridium Anticancer Complexes. *J. Med. Chem.* **2011**, *54*, 3011−3026.
(21) For ethacrynic acid: (a) Wang, R.; Li, C.; Song, D.; Zhao, G.; Zhao, L.; Jing, Y. Ethacrynic Acid Butyl-Ester Induces Apoptosis in Leukemia Cells through a Hydrogen Peroxide−Mediated Pathway Independent of Glutathione S-Transferase P1−1 Inhibition. *Cancer Res.* **2007**, *67*, 7856−7564. (b) Agonigi, G.; Riedel, T.; Pilar Gay, M.; Biancalana, L.; Oñate, E.; Dyson, P. J.; Pampaloni, G.; Paunescu, E.; Esteruelas, M. A.; Marchetti, F. Arene Osmium Complexes with Ethacrynic Acid-Modified Ligands: Synthesis, Characterization, and Evaluation of Intracellular Glutathione S-Transferase Inhibition and Antiproliferative Activity. *Organometallics* **2016**, *35*, 1046−1056. (c) Mignani, S.; El Brahmi, N.; El Kazzouli, S.; Eloy, L.; Courilleau, D.; Caron, J.; Bousmina, M. M.; Caminade, A.-M.; Cresteil, T.; Majoral, J.-P. A novel class of ethacrynic acid derivatives as promising drug-like potent generation of anticancer agents with established mechanism of action. *Eur. J. Med. Chem.* **2016**, *122*, 656−673.
(22) (a) Schmitt, F.; Kasparkova, J.; Brabec, V.; Begemann, G.; Schobert, R.; Biersack, B. New (arene)ruthenium(II) complexes of 4-aryl-4H-naphthopyrans with anticancer and anti-vascular activities. *J. Inorg. Biochem.* **2018**, *184*, 69. (b) Novohradsky, V.; Zerzankova, L.; Stepankova, J.; Kisova, A.; Kostrhunova, H.; Liu, Z.; Sadler, P. J.; Kasparkova, J.; Brabec, V. A dual-targeting, apoptosis-inducing organometallic half-sandwich iridium anticancer complex. *Metallomics* **2014**, *6*, 1491−501.
(23) Ethacrynic acid (CAS 58-54-8): 2,3-dichloro-4-(2-methylene-1-oxobutyl)phenoxyacetic acid. Flurbiprofen (CAS 5104-49-4): (±)-2-fluoro-α-methyl-(1,1′-biphenyl)-4-acetic acid (racemic mixture). Biotin (CAS 58-85-5): 5-[(3a*S*,4*S*,6a*R*)-2-oxohexahydro-1*H*-thieno[3,4-*d*]imidazol-4-yl]pentanoic acid. Potassium benzylpenicillin (CAS 113-98-4): potassium (2*S*,5*R*,6*R*)-3,3-dimethyl-7-oxo-6-[(phenylacetyl) amino]-4-thia-1-azabicyclo[3.2.0]heptane-2-carboxylate.
(24) (a) Bennett, M. A.; Smith, A. K. Arene ruthenium(II) complexes formed by dehydrogenation of cyclohexadienes with ruthenium(III) trichloride. *J. Chem. Soc., Dalton Trans.* **1974**, 233−241. (b) Optimized procedure: Biancalana, L.; Zacchini, S.; Ferri, N.; Lupo, M. G.; Pampaloni, G.; Marchetti, F. Tuning the cytotoxicity of ruthenium(II) para-cymene complexes by mono-substitution at a triphenylphosphine/phenoxydiphenylphosphine ligand. *Dalton Trans.* **2017**, *46*, 16589−16604.
(25) White, C.; Yates, A.; Maitlis, P. M. ($\eta^5$-pentamethylcyclopentadienyl)rhodium and -iridium compounds. *Inorg. Synth.* **2007**, *29*, 228−234.
(26) Fulmer, G. R.; Miller, A. J. M.; Sherden, N. H.; Gottlieb, H. E.; Nudelman, A.; Stoltz, B. M.; Bercaw, J. E.; Goldberg, K. I. NMR Chemical Shifts of Trace Impurities: Common Laboratory Solvents, Organics, and Gases in Deuterated Solvents Relevant to the Organometallic Chemist. *Organometallics* **2010**, *29*, 2176−2179.
(27) Harris, R. K.; Becker, E. D.; Cabral De Menezes, S. M.; Goodfellow, R.; Granger, P. NMR nomenclature. Nuclear spin properties and conventions for chemical shifts (IUPAC Recommendations 2001). *Pure Appl. Chem.* **2001**, *73*, 1795−1818.
(28) Willker, W.; Leibfritz, D.; Kerssebaum, R.; Bermel, W. Gradient selection in inverse heteronuclear correlation spectroscopy. *Magn. Reson. Chem.* **1993**, *31*, 287−292.
(29) Menges, F. *Spectragryph-optical spectroscopy software, Ver. 1.2.14d*, 2016−2020; http://www.effemm2.de/spectragryph.
(30) A solution of $[IrCl_2(\eta^5\text{-}C_5Me_5)]_2$ (29 mg, 0.036 mmol) in MeOH (5 mL) was treated with $AgNO_3$ (12 mg, 0.073 mmol) and stirred at room temperature in the dark. After 1 h, the mixture was filtered over a celite pad and $\mathbf{L}^{EB}$ (66 mg, 0.078 mmol) was added to the yellow filtrate solution. The suspension was stirred at reflux for 15 h, affording an orange solution. NMR analysis ($^{1}$H, $CDCl_3$) revealed a mixture of $[\mathbf{6}]^+$, ***B*-CO$_2$(CH$_2$)$_2$OH**, ***E*-CO$_2$(CH$_2$)$_2$OH**, and ***E*-CO$_2$H** (1:1:0.8:0.2 molar ratio).
(31) Sheldrick, G. M. *SADABS-2008/1 - Bruker AXS Area Detector Scaling and Absorption Correction*; Bruker AXS: Madison, WI, USA, 2008.
(32) Sheldrick, G. M. Crystal Structure Refinement with SHELXL. *Acta Crystallogr., Sect. C: Struct. Chem.* **2015**, *71*, 3−8.
(33) Rundlöf, T.; Mathiasson, M.; Bekiroglu, S.; Hakkarainen, B.; Bowden, T.; Arvidsson, T. Survey and qualification of internal standards for quantification by 1H NMR spectroscopy. *J. Pharm. Biomed. Anal.* **2010**, *52*, 645−651.
(34) $^{14}$N and $^{35}$Cl NMR reference data. All data refer to the pure compounds dissolved in the selected solvent. NaCl: $^{35}$Cl NMR ($8.8 \times 10^{-2}$ M, DMSO/$H_2O$ 5/1, few scans): $\delta$/ppm 44.6 ($\Delta\nu_{1/2}$ = 545 Hz). KCl: $^{35}$Cl NMR ($1.9 \times 10^{-2}$ M, DMSO/$H_2O$ 5/1, few scans): $\delta$/ppm 41.2 ($\Delta\nu_{1/2}$ = 447 Hz). $NaNO_3$: $^{14}$N NMR (DMSO/$H_2O$ 5/1): $\delta$/ppm −5.1 ($\Delta\nu_{1/2}$ = 23 Hz).
(35) Mosmann, T. Rapid colorimetric assay for cellular growth and survival: application to proliferation and cytotoxicity assays. *J. Immunol. Methods* **1983**, *65*, 55−63.


https://doi.org/10.1021/acs.inorgchem.1c00641
*Inorg. Chem.* 2021, 60, 9529−9541